

4

AD-A216 637

GL-TR-89-0175  
ENVIRONMENTAL RESEARCH PAPERS, NO. 1033

# Comparisons Between the RTNEPH and AFGL Cloud Layer Analysis Algorithms

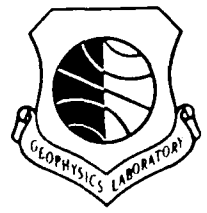
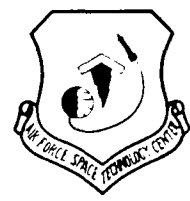
ROBERT P. d'ENTREMONT  
GARY B. GUSTAFSON  
JAMES T. BUNTING  
MICHAEL K. GRIFFIN  
CRYSTAL BARKER SCHAAF  
PAMELA L. NOWAK  
JOAN M. WARD  
RUPERT S. HAWKINS



15 July 1989



Approved for public release; distribution unlimited.



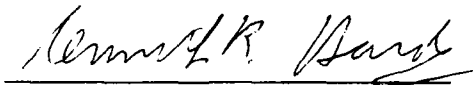
ATMOSPHERIC SCIENCES DIVISION PROJECT 6670

**GEOPHYSICS LABORATORY**  
HANSCOM AFB, MA 01731-5000

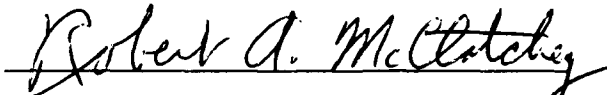
90 01 16 123

"This technical report has been reviewed and is approved for publication."

FOR THE COMMANDER,



KENNETH R. HARDY, Chief  
Satellite Meteorology Branch



ROBERT A. McCLATCHEY, Director  
Atmospheric Sciences Division

This document has been reviewed by the ESD Public Affairs Office (ESD/PA) and is releasable to the National Technical Information Service (NTIS).

Qualified requestors may obtain additional copies from the Defense Technical Information Center. All others should apply to the National Technical Information Service.

If your address has changed, or if you wish to be removed from the mailing list, or if the addressee is no longer employed by your organization, please notify AFGL/DAA, Hanscom AFB, MA 01731-5000. This will assist us in maintaining a current mailing list.

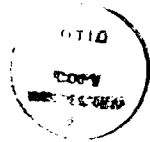
Do not return copies of this report unless contractual obligations or notices on a specific document require that it be returned.

Unclassified

SECURITY CLASSIFICATION OF THIS PAGE

**REPORT DOCUMENTATION PAGE**

1a. REPORT SECURITY CLASSIFICATION Unclassified		1b. RESTRICTIVE MARKINGS	
2a. SECURITY CLASSIFICATION AUTHORITY		3. DISTRIBUTION/AVAILABILITY OF REPORT Approved for public release; distribution unlimited.	
2b. DECLASSIFICATION/DOWNGRADING SCHEDULE		5. MONITORING ORGANIZATION REPORT NUMBER(S)	
4. PERFORMING ORGANIZATION REPORT NUMBER(S) GL-TR-89-0175 ERP, No. 1033		7a. NAME OF MONITORING ORGANIZATION	
6a. NAME OF PERFORMING ORGANIZATION Geophysics Laboratory	6b. OFFICE SYMBOL (if applicable) LYS	7b. ADDRESS (City, State, and ZIP Code)	
6c. ADDRESS (City, State, and ZIP Code) Hanscom AFB Massachusetts 01731-5000		9. PROCUREMENT INSTRUMENT IDENTIFICATION NUMBER	
8a. NAME OF FUNDING/SPONSORING ORGANIZATION	8b. OFFICE SYMBOL (if applicable)	10. SOURCE OF FUNDING NUMBERS	
8c. ADDRESS (City, State, and ZIP Code)		PROGRAM ELEMENT NO. 62101F	PROJECT NO. 6670
		TASK NO. 17	WORK UNIT ACCESSION NO. 07
11. TITLE (Include Security Classification) <b>Comparisons Between the RTNEPH and AFGL Cloud Layer Analysis Algorithms</b>			
12. PERSONAL AUTHOR(S) Robert P. d'Entremont, Gary B. Gustafson*, James T. Bunting, Michael K. Griffin, Crystal Barker Schaaf, Pamela L. Nowak**, Joan M. Ward+ Rupert S. Hawkins			
13a. TYPE OF REPORT Scientific	13b. TIME COVERED FROM TO	14. DATE OF REPORT (Year, Month, Day) 1989 July 15	15. PAGE COUNT 70
16. SUPPLEMENTARY NOTATION* Atmospheric & Environmental Research Inc, 840 Memorial Drive, Cambridge MA 02139; ** Dynamic Research Corp, 60 Concord St, Wilmington, MA 01887; + System Resources Corp, 128 Wheeler Road, Burlington, MA 01803			
17. COSATI CODES		18. SUBJECT TERMS (Continue on reverse if necessary and identify by block number)	
FIELD	GROUP	Cloud Analysis	
		Infrared Imagery	
		Satellite Imagery	
		Cloud Layers	
19. ABSTRACT (Continue on reverse if necessary and identify by block number) The Real-Time Nephanalysis (RTNEPH) is an automated cloud analysis model in operational use at the Air Force Global Weather Central (AFGWC). In the RTNEPH, polar-orbiting satellite imagery is analyzed in conjunction with conventional meteorological cloud observations to produce a global analysis of cloud attributes such as extent, height, bases, and type. In 1980, an alternative to the RTNEPH layer analysis algorithm was developed at the Air Force Geophysics Laboratory (AFGL). The AFGL algorithm performs a layer analysis using a 16 x 16 array of IR satellite pixels, four times larger than the RTNEPH array size. The AFGL cloud layer algorithm was proposed as an alternative to the current RTNEPH algorithm. This report describes the comparison study that was conducted on the AFGL and RTNEPH cloud layer algorithms and characterizes their differences in terms of the key meteorological parameters. The report contains recommendations for incorporating the AFGL algorithm into the RTNEPH and suggestions for future work in this area.			
20. DISTRIBUTION/AVAILABILITY OF ABSTRACT <input type="checkbox"/> UNCLASSIFIED/UNLIMITED <input type="checkbox"/> SAME AS RPT <input type="checkbox"/> DTIC USERS		21. ABSTRACT SECURITY CLASSIFICATION Unclassified	
22a. NAME OF RESPONSIBLE INDIVIDUAL Robert P. d'Entremont		22b. TELEPHONE (Include Area Code) (617) 377-2983	22c. OFFICE SYMBOL GL/LYS



Accession For	
NTIS GRA&I	<input checked="" type="checkbox"/>
DTIC TAB	<input type="checkbox"/>
Unannounced	<input type="checkbox"/>
Justification	
By	
Distribution/	
Availability Codes	
Avail and/or	
Dist	Special
A-1	

... ..  
... ..  
... ..  
... ..

DISTRIBUTION STATEMENT A
Approved for public release
Distribution Unlimited

## Contents

1. INTRODUCTION	1
2. THE AFGWC REAL-TIME NEPHANALYSIS	3
2.1 The Infrared Satellite Data Processor	3
2.1.1 RTNEPH IR Cloud/No-Cloud Decisions	4
2.1.2 Determination of Cloud Layers	5
2.1.3 Determination of Cloud Amounts and Heights	7
3. THE AFGL RESEARCH AND DEVELOPMENT NEPHANALYSIS	7
3.1 AFGL RDNEPH Data Processing Design	8
3.1.1 RDNEPH Supporting Data Bases	9
3.1.2 Eighth-mesh Processing Flags	11
4. COMPARISON RESULTS	12
4.1 Representative Grayshade Images	12
4.2 RDNEPH Statistics	13
4.3 Cloud Truth Images	17
5. DISCUSSION	24
5.1 Cloud Layers	24
5.2 Cloud Heights	28
6. CONCLUSIONS AND RECOMMENDATIONS	33
7. RTNEPH HEMISPHERIC DATABASE DISPLAYS	35
8. RTNEPH AND AFGL CLOUD ANALYSIS STATISTICS	49
REFERENCES	61

## Illustrations

1.	Example of a Grayshade Histogram	6
2.	Plot of Average Cloud Amount Per Layer for the RTNEPH and AFGL Algorithms	15
3.	Sample Plot of the Frequency Distribution of Number of Layers for the RTNEPH and AFGL Algorithms	16
4.	Sample Plot of the Frequency Distribution of Total Cloud Amount	17
5.	Sample Plot of Total Cloud Amount vs. Viewing Angle	17
6a.	RGS Image for RTNEPH Box 45, Summer Day 82162	20
6b.	Cloud Truth Image for RTNEPH Box 45, Summer Day 82162	21
6c.	Visible Image for RTNEPH Box 45, Summer Day 82162	22
6d.	Infrared Image for RTNEPH Box 45, Summer Day 82162	23
7.	Plots of Layer Frequency as a Function of Number of Cloud Layers for the RTNEPH and AFGL Algorithms (See Tables 3 and 4 Layer Frequency Statistics)	27
8.	Plots of Hemispheric Cloud Layer Distributions and Average Layer Cloud Amounts as a Function of Height for the RTNEPH Algorithm, Summer Day 82162 (See Table 13)	30
9.	Plots of Hemispheric Cloud Layer Distributions and Average Layer Cloud Amounts as a Function of Height for the AFGL Algorithm, Summer Day 82162 (See Table 14)	31
10.	Plots of Hemispheric Cloud Layer Distributions and Average Layer Cloud Amounts as a Function of Height for the RTNEPH Algorithm, Winter Day 85009 (See Table 15)	32
11.	Plots of Hemispheric Cloud Layer Distributions and Average Layer Cloud Amounts as a Function of Height for the AFGL Algorithm, Winter Day 85009 (See Table 16)	33
12.	Northern Hemisphere Terrain Heights (See Section 3.1.1, Page 9)	37
13.	Geography Flags for the Summer And Winter Case Study Days (See Section 3.1.1, Page 9)	38
14a.	Background Brightness for the Summer Day 82162 (See Section 3.1.1, Page 10)	39

14b.	Background Brightness for the Winter Day 85009 (See Section 3.1.1, Page 10)	40
15a.	Composite Surface Temperature Field for the Summer Case Study Day 82162 (See Section 3.1.1, Page 11)	41
15b.	Three-hourly Surface Temperature Fields for the Winter Case Study Day 85009 (See Section 3.1.1, Page 11)	42
15c.	Composite Surface Temperature Field for the Winter Case Study Day 85009 (See Section 3.1.1, Page 11)	43
16.	Infrared Satellite Global Data Base Image for the Summer Case Study Day 82162 (See Section 3.1.2, Page 12)	44
17.	Hemispheric Representative Grayshade Image for the Summer Case Study Day 82162 (See Section 4.1, Page 13)	45
18.	Infrared Satellite Global Data Base Image for the Winter Case Study Day 85009 (See Section 3.1.2, Page 12)	46
19.	Hemispheric Representative Grayshade Image for the Winter Case Study Day 85009 (See Section 4.1, Page 13)	47

## Tables

1.	RTNEPH Grid Sizes	8
2.	Representative Grayshade Values	14
3.	IR Processor Hemispheric Statistics for the Summer Case Study Day 82162	25
4.	IR Processor Hemispheric Statistics for the Winter Case Study Day 85009	26
5.	Altitude Ranges for the Layers of the 5LAYER Cloud Forecast Model	29
6.	Latitude Bounds for the Tropics, Mid-latitudes, and Polar Regions for the Summer and Winter Case Study Days	29
7.	Hemispheric Cloud Statistics for 82162, Low Clouds (See Section 5.1, Page 27)	50

8.	Hemispheric Cloud Statistics for 82162, Middle Clouds (See Section 5.1, Page 27)	51
9.	Hemispheric Cloud Statistics for 82162, High Clouds (See Section 5.1, Page 27)	52
10.	Hemispheric Cloud Statistics for 85009, Low Clouds (See Section 5.1, Page 27)	53
11.	Hemispheric Cloud Statistics for 85009, Middle Clouds (See Section 5.1, Page 27)	54
12.	Hemispheric Cloud Statistics for 85009, High Clouds (See Section 5.1, Page 27)	55
13.	Cloud Layer Distribution and Average Layer Cloud Amounts for the RTNEPH Algorithm, Day 82162 (See Figure 8)	56
14.	Cloud Layer Distribution and Average Layer Cloud Amounts for the AFGL Algorithm, Day 82162 (See Figure 9)	57
15.	Cloud Layer Distribution and Average Layer Cloud Amounts for the RTNEPH Algorithm, Day 85009 (See Figure 10)	58
16.	Cloud Layer Distribution and Average Layer Cloud Amounts for the AFGL Algorithm, Day 85009 (See Figure 11)	59

# Comparisons Between the RTNEPH and AFGL Cloud Layer Analysis Algorithms

## 1. INTRODUCTION

The Real-Time Nephanalysis (RTNEPH) is an automated cloud analysis model that is in operational use at the Air Force Global Weather Central (AFGWC). In the RTNEPH, polar-orbiting satellite imagery is analyzed in conjunction with conventional meteorological cloud observations to produce a global analysis of cloud attributes such as extent, height, bases, and type. The RTNEPH and its predecessor, the Three-Dimensional Nephanalysis (3DNEPH), have been generating real-time global cloud analyses since 1970 (see Fye, 1978; Kiess and Cox, 1988). RTNEPH cloud analyses are used primarily to initialize cloud forecast models in support of Air Force missions, and they are also archived for use by the research community as one of the few sources of long-term global cloud climatologies available today.

Infrared (IR) satellite imagery is the primary and most reliable source of global cloud observations for the RTNEPH because of the frequent updates and availability of the data both day and night. The RTNEPH infrared processor makes cloud cover decisions by comparing measured IR brightness temperatures with an expected underlying surface temperature. Simply stated, if the measured brightness temperature (with atmospheric effects removed) is sufficiently colder than the underlying surface temperature, cloud is detected.

The RTNEPH contains a layer analysis algorithm that combines pixels of an  $8 \times 8$  IR satellite image into thermally homogeneous groups. These groups, referred to as clusters, form the basis of the RTNEPH cloud layer analysis.

---

Received for Publication - 29 June 1989



In 1980, an alternative to the RTNEPH layer analysis algorithm was developed at the Air Force Geophysics Laboratory (AFGL). The AFGL algorithm (see Hawkins, 1980; 1981) performs a layer analysis using a  $16 \times 16$  array of IR satellite pixels, four times larger than the RTNEPH array size. An early comparison study (d'Entremont et al., 1982) showed that the AFGL algorithm produces a more realistic result because of the additional cloud information contained in the larger array. This result is obtained even though the AFGL algorithm is no more computationally complex than the RTNEPH layer analysis algorithm. As a result of the positive conclusions of the early study, the AFGL cloud layer algorithm was proposed as an alternative to the current RTNEPH algorithm.

Although a limited comparison had already been performed between the AFGL and the 3DNEPH layer algorithm (d'Entremont et al., 1982), the Air Weather Service requested that another more comprehensive comparison study be conducted using the RTNEPH algorithm. In response to that request AFGL, in collaboration with the RTNEPH software group, developed test procedures for a new comparison study.

The comparison was performed using case study days. Two days were selected as representative of a wide variety of conditions; one from the summer (11 June 1982, Julian date 82162) and one from the winter (9 January 1985, Julian date 85009). AFGL had all the data necessary to perform a hemispheric nephanalysis for both days. The data had been obtained earlier from AFGWC through periodic data saves that were made specifically for AFGL nephanalysis investigations (Bunting et al., 1983). For each of the case study days, two full hemispheric cloud analyses were generated using the RTNEPH and the AFGL cloud layer algorithms respectively. Results of the separated analyses were compared visually and statistically to characterize the differences.

All work for the comparison study was performed on the AFGL Interactive Meteorological Computer System (AIMS). AIMS is a distributed system of mini- and microcomputers and special purpose imaging computers, all linked by a local area network (for a system description see Gustafson, et al., 1987). AIMS is ideally suited for this type of investigation because of the amount of mass storage available for the large RTNEPH data bases, the inherently interactive hands-on nature of the system, and its extensive image processing capabilities.

This report describes the comparison study conducted on the two cloud layer algorithms and characterizes their differences in terms of the key meteorological parameters. The report concludes with recommendations for incorporating the AFGL algorithm into the RTNEPH and with suggestions for future work in this area.

## 2. THE AFGWC REAL-TIME NEPHANALYSIS

RTNEPH is the operational realtime cloud analysis model of the Air Force. It is composed of four primary modules: the satellite, conventional, merge, and bogus processors. Each performs a major function in the analysis of available cloud observation data.

The satellite processor generates a cloud analysis that is derived from satellite observations of cloud cover. Two non-satellite supporting databases required are conventional meteorological observations of surface temperatures and upper-air temperature profiles. These data are used by the satellite processor for cloud detection and to assign cloud top altitudes. The satellite processor analyzes both visible and infrared data. In general, the darker a visible grayshade value is, the less cloud there is associated with that grayshade. Conversely, the higher an IR brightness temperature is, the more likely it is to represent a cloud-free area.

The conventional processor generates a separate cloud analysis that is derived solely from surface, rawinsonde, and aircraft pilot observations of cloud cover and weather.

Both the satellite and conventional processors generate an individual cloud analysis for only those gridpoints where each has processed data. The two analyses are subsequently combined by the merge processor where they are subjected to stringent timeliness and quality checks (Kiess and Cox, 1988). The combining of these two databases is the major step in producing the final RTNEPH operational cloud analysis.

The bogus processor permits interactive modification of the merge processor analysis. Manual corrections can be made at locations where the analysis is interpreted as unrepresentative of actual conditions. This judgement is most often based on subjective interpretation of fine-resolution satellite imagery valid for the analysis time and area.

The satellite processor analysis dominates the merged, pre-bogused cloud analysis since satellite data are the only true source of global cloud cover observations available to the RTNEPH. Infrared data are the most frequently processed satellite data because they are available day and night, and their use is not complicated by changes in solar viewing geometry. For these reasons AFGL devotes its nephanalysis efforts primarily to studies of the IR processor, although future plans include studies of the visible processor.

### 2.1 The Infrared Satellite Data Processor

The infrared satellite processor generates a cloud analysis that is derived from IR satellite observations of cloud cover. These IR data are stored in a regular grid known as the Satellite Global Data Base (SGDB); there is also corresponding visible

data in the SGDB. Satellite data are mapped into the SGDB as soon as they become available. The nominal resolution of a pixel within the SGDB is 3 n mi. The RTNEPH IR processor produces a cloud analysis over an  $8 \times 8$  array of IR pixels.

The infrared processor has three main functions: 1) select a cutoff IR grayshade that delineates cloudy pixels from clear pixels; 2) perform a layer analysis on the cloudy pixels; and 3) determine the resultant cloud parameters. Each of these steps is outlined in the following sections.

### 2.1.1 RTNEPH IR CLOUD/NO-CLOUD DECISIONS

IR grayshades in the SGDB represent specific temperature ranges. The relation between grayshade and temperature is linear: grayshades range from 0 (dark) to 63 (bright) and correspond to temperatures from 310 K to 190 K, respectively. This relationship between grayshade and temperature is chosen so that when the grayshades are displayed, bright grayshades denote clouds while dark grayshades denote clear areas. At AFGWC, this convention is inverted: 0 corresponds to 190 K and 63 corresponds to 310 K.

Consider an  $8 \times 8$  array comprised of clear and cloudy pixels, each represented by some grayshade  $G$ . The selection of a cloud/no-cloud cutoff that separates the clear and the cloudy grayshades is first made by determining the measured temperature  $T_{\text{obs}}(G)$  of the scene being viewed via lookup tables. Then  $T_{\text{obs}}$  and the underlying surface temperature  $T_{\text{sfc}}$  are compared, where  $T_{\text{sfc}}$  is the temperature that the satellite measures if the scene is cloud-free.

In an ideal situation, if the difference

$$\Delta T_{\text{obs}} = T_{\text{sfc}} - T_{\text{obs}} \quad (1)$$

is greater than zero, the pixel represented by  $T_{\text{obs}}$  is cloudy since the scene being viewed has a lower temperature than the underlying surface. (This assumes that atmospheric temperature monotonically decreases with height.) If  $\Delta T_{\text{obs}}$  is less than or equal to 0, then the scene is clear.

However, biases are present in the IR temperature measurements. There are also uncertainties in the accuracy of the surface temperatures that the RTNEPH uses, and atmospheric water vapor attenuation cannot be neglected. These issues complicate the cloud/no-cloud decision defined by the simple scenario outlined in Eq. (1) above. In the RTNEPH, correction factors are applied to the measured IR temperature  $T_{\text{obs}}$ . These corrections are a function of: 1) satellite sensor, to account for any biases inherent in the sensor construction that affect its measurements; 2) geography type and time of day, to account for uncertainties in how well the surface temperature  $T_{\text{sfc}}$  represents the background skin temperature; and 3) earth location, since water vapor attenuation corrections are made for tropical regions.

The reliability of the surface temperature values is of concern. Surface temperature fields that are used for data-sparse regions have higher uncertainties than those collected in data-rich regions. It is because of this uncertainty that, instead of being greater than or equal to zero,  $\Delta T_{\text{obs}}$  must be greater than or equal to some cloud threshold value  $\Delta T_{\text{cld}}$  before the RTNEPH detects cloud.  $\Delta T_{\text{cld}}$  is typically nonzero, varies with earth location, and is higher for data-sparse regions of the globe than it is for data-rich regions. A higher threshold  $\Delta T_{\text{cld}}$  forces a measured IR temperature  $T_{\text{obs}}$  to be considerably lower than the surface temperature before cloud is detected. In other words, extra precaution is taken in data-sparse regions to ensure that an incorrect cloud decision is not made.

In summary, RTNEPH considers a given scene to be cloudy when the temperature  $T_{\text{obs}}$  of that scene satisfies the condition

$$\Delta T_{\text{obs}} \geq \Delta T_{\text{cld}}, \quad (2)$$

where  $\Delta T_{\text{obs}}$  is given by Eq. (1) with  $T_{\text{obs}}$  corrected for bias and atmospheric effects, and where  $\Delta T_{\text{cld}}$  is a predetermined function of earth location and time of day.

### 2.1.2 DETERMINATION OF CLOUD LAYERS

Having separated out the cloudy pixels using Eq. (2), the remaining clear pixels are excluded from any further cloud processing. The cloudy pixels are then analyzed for cloud layers. The RTNEPH uses a layer analysis algorithm that processes a maximum array size of  $8 \times 8$ ; the AFGL layer algorithm processes a  $16 \times 16$  array.

Although they process different array sizes, each algorithm starts its analysis in essentially the same way. From the original array of IR data a grayshade distribution, called a histogram, is constructed using only the cloudy grayshades. Histograms typically show peaks and valleys that in theory separate one cloud layer from the next. An example of a histogram is shown in Figure 1.

When looking at the histogram it is sometimes easy to see in a subjective sense where one cloud layer ends and another begins, while at other times it is not so easy. The job of the RTNEPH and AFGL layer algorithms is to objectively determine where the layer grayshade boundaries are, and to pass this information on to the part of the IR processor that determines layer cloud top heights and amounts.

There are subtle, persistent differences in the way that each algorithm performs. The objective rules that each algorithm invokes in determining layer boundaries are not the same. How these differences manifest themselves in the final IR processor output is the major issue addressed in this paper. Detailed outlines of how each algorithm works are beyond the scope of this paper. Readers who want more information about the AFGL algorithm should refer to Hawkins (1980, 1981), and for the RTNEPH algorithm, to Kiess and Cox (1988).

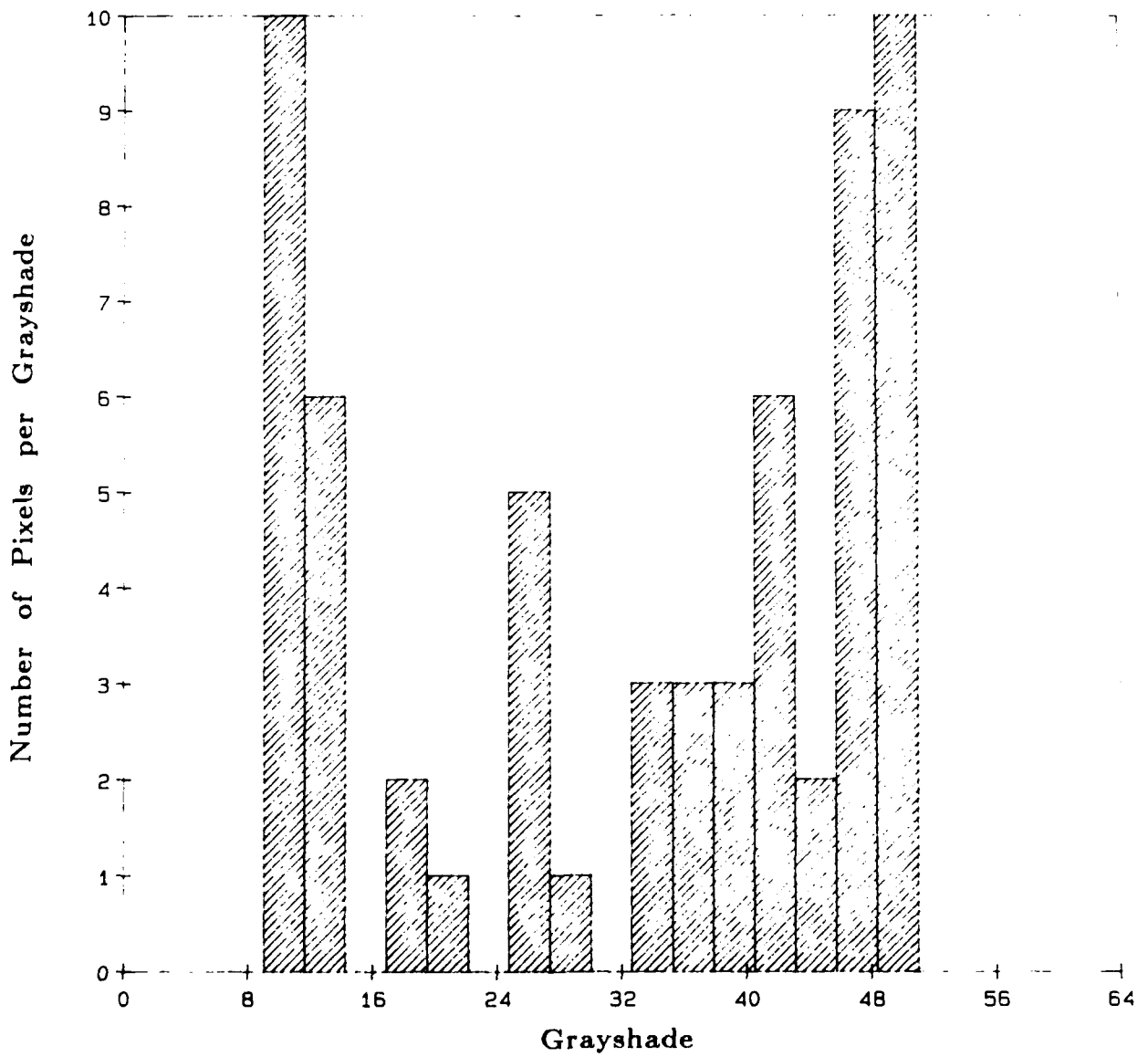


**Figure 1.** Example of a Grayshade Histogram. The First Layer (Cluster) Lies Between Grayshade Values 8 and 16, the Second Between 17 and 32, and the Third Between 33 and 50

### 2.1.3 DETERMINATION OF CLOUD AMOUNTS AND HEIGHTS

Once layer grayshade boundaries are specified, the cloud amount for that layer is computed by: 1) counting the number of pixels with grayshade values that fall between the given layer boundaries; and 2) dividing that count by the total number of pixels within the analysis array. In order to compute the layer top height, the brightest IR grayshade (coldest cloud top) for the layer is first converted to cloud top temperature using the lookup table (see Section 2.2). This temperature is then corrected for atmospheric attenuation and satellite sensor biases before it is used to calculate a cloud height using the temperature-height profile valid for the location being analyzed.

## 3. THE AFGL RESEARCH AND DEVELOPMENT NEPHANALYSIS

The AFGL research and development nephanalysis (RDNEPH) is the baseline program that is used to test both the RTNEPH and AFGL cloud algorithms in a consistent environment. RDNEPH has four functions: 1) accept user processing instructions; 2) access the satellite and supporting data from the AFGL data base that are required to perform the cloud analysis; 3) invoke either the RTNEPH or the AFGL algorithm, and; 4) generate results in the form of representative grayshade (RGS) displays and tabular listings of total cloud, cloud amount and height by layer, and various processing parameters and statistics. RGS displays are synthetic images that are produced from interim results of both nephanalysis programs. The images are used extensively at AFGL for evaluation (see Section 4.1).

Significant differences exist between the RDNEPH framework and that of the RTNEPH. However, considerable care was exercised to insure that both processing algorithms operate in exactly the same way within RDNEPH as they do at AFGWC. Only changes that were necessitated by the vast differences in computing environments between AFGWC and AFGL were made to the processing algorithms. When setting up the test environment, data base considerations were minimized by the decision to retain the AFGWC NEPH grid structure for use at AFGL. The NEPH grid structure is used operationally at AFGWC to manage all input and output data associated with the RTNEPH. It consists of a series of nested grids mapped to a hemispheric standard polar stereographic projection true at 60° latitude. The center of the projection is at the pole, and the horizontal axis is aligned with the 10° east meridian. Varying grid resolutions are computed as fractions of the standard mesh size of 200 n mi, known as whole-mesh. Resolution increases by factors of two (that is, 2, 4, 8, 16...) and the gridpoints are referred to respectively as half-mesh boxes, quarter-mesh boxes, eighth-mesh boxes, sixteenth-mesh boxes, etc. Table 1

<b>Grid Resolutions and Databases of the RTNEPH</b>		
<i>Grid Size</i>	<i>Nominal Resolution (True at 60 °)</i>	<i>Types of Data Available at This Resolution</i>
RTNEPH Box	1600 n mi	Standard Block of Cloud Analysis
Whole-mesh	200 n mi	Upper Air Temperature Profiles
Quarter-mesh	50 n mi	Satellite Times and Viewing Angles
Eighth-mesh	25 n mi	Cloud Cover Analysis; Surface Temperatures; Terrain Heights; Geography; Background Brightness
Sixty-fourth- mesh	3 n mi	Satellite Data in the SGDB

**Table 1.** Resolutions of the RTNEPH Grid Structure. Examples of RTNEPH Databases That Have Resolutions at Each Grid Size Are Also Listed

lists the grid resolutions used by the RTNEPH data base (see Hoke et al. (1981) for a complete description of the NEPH grid structure). It should be noted that the  $8 \times 8$  array used by the RTNEPH algorithm corresponds exactly to one eighth-mesh box of satellite data, while the  $16 \times 16$  AFGL array is one quarter-mesh box.

### 3.1 AFGL RDNEPH Data Processing Design

The AFGWC RTNEPH accesses many dynamic data bases in realtime. Both the data sources and their valid times vary significantly. Because it runs in realtime the RTNEPH must constantly interpolate supporting data to the times of the satellite data before they can be used in the cloud analysis. However, the AFGL RDNEPH has no realtime constraints, making time-interpolation during execution unnecessary. Free of this constraint, AFGL was able to simplify the complex data management functions of the RDNEPH code by performing the necessary time-interpolations *prior* to runtime.

An AFGL RDNEPH data field represents the most up-to-date surface or atmospheric conditions available at the time of the satellite data save. Each particular type of RDNEPH data contains the pertinent and most timely parts of several AFGWC data fields. Among the RTNEPH data bases that change with time are background brightness, surface temperature, and atmospheric temperature and height profiles in addition to the visible and infrared satellite data. Terrain heights and geography flags require no time-interpolation for the RDNEPH.

Full-page color enhanced displays of each hemispheric database are in Section 7,

Figures 12 - 19. Since each display takes up almost a full page, it is less disruptive to the reader and easier to compare the displays with one another when they are placed together away from the main text. All the figures in Section 7 are cited in the following sections. A description follows of each of the RDNEPH databases.

### 3.1.1 RDNEPH SUPPORTING DATA BASES

**Surface Terrain Height.** Surface terrain heights are provided for each eighth-mesh gridpoint, and have a 10 m vertical resolution. Terrain heights are used to ensure that analyzed cloud layer base and height altitudes are not below ground level. Since terrain heights remain essentially unchanged with time, the terrain field for the two test dates are identical. Figure 12 shows the northern hemisphere terrain data base.

**Geography Flags.** Like the terrain data, the geography flags are also provided for every eighth-mesh gridpoint. Geography flags indicate whether an eighth-mesh box is composed predominantly of water, land, ice, coastline, or if the box is off-hemisphere (as far as the grid projection is concerned). These flags play a role in determining corrections to measured IR brightness temperatures.

In the absence of clouds, IR sensors measure the temperature of the Earth's surface. However, for land backgrounds the surface temperature database contains shelter temperatures (that is, the temperature of the air a few meters above the ground). Therefore, to accurately detect cloud, the threshold algorithm ( Eq. (2) ) must first modify the shelter temperatures to compensate for differences that exist between the temperature of the air and the underlying surface. These corrections are applied as a function of geography type. Typically they are larger for land backgrounds than for water backgrounds, since over the oceans the surface temperature database contains temperatures that are very close to actual sea surface temperatures. The corrections also vary with time of day.

Since geography fields contain sea ice-cover information, they vary from week to week. Figure 13 shows the geography data for the summer and winter case study days, with the seasonal differences in sea-ice coverage highlighted.

**Background Brightness.** Background brightness is defined as the brightest visible SGDB grayshade value that a pixel within a particular eighth-mesh box is expected to have when the pixel is cloud-free. In the visible satellite data processor, measured visible grayshade values are compared against the expected background brightness value to determine whether clouds are present in the scene. If the measured pixel value is higher than the background value by a pre-specified threshold amount, the pixel is cloudy; if the pixel value is lower, the pixel is cloud-free.

Background brightness values are used by the nephanalysis IR processor to help determine the magnitude of the cloud IR threshold (see Section 2.1.1). In general, the higher the background brightness value (that is, the more reflective the background),



the greater the clear/cloud temperature threshold. In other words, observed IR brightness temperatures must be lower than the underlying surface temperature by a larger amount for brighter surfaces than for darker surfaces before the nephanalysis will detect cloud. The reason is that bright, highly reflective cloud-free surfaces tend to be deserts or other remote regions with high diurnal temperature ranges and very few observations of surface temperature. Surface temperature fields that are used for these data-sparse regions have higher uncertainties than those collected in data-rich regions. Adjusting the clear/cloud threshold higher reflects this uncertainty, since the higher value forces an IR temperature to be definitively lower than the background skin temperature before cloud is detected.

The background brightness field is a dynamic database that is monitored and updated by the RTNEPH in real-time. There is one database per satellite. Updates in background brightness values are necessary due to changes in snow/ice cover and vegetation (week-to-week variations), solar declination (seasonal variations), and other natural effects. Figures 14a and 14b contain the background brightness fields for the two case study days. Land background brightnesses are depicted as either a shade of green (lower albedoes) or yellow (higher albedoes; note especially the deserts). Separate background brightness values are used for snow, ice and water. Eighth-mesh boxes that contain snow cover are represented by white pixels, along with ice and water flags (gray and blue, respectively) merged in from the geography data base.

In Figure 14a, problems with snow coverage at lower latitudes are readily apparent for the summer day 82162. This problem is less evident for the winter day 85009 shown in Figure 14b. These inaccuracies can adversely affect the clear/cloud decisions of the visible and IR processors.

**Surface Temperatures.** Surface temperatures are available at eighth-mesh resolution. In the nephanalysis, if the IR brightness temperature is sufficiently lower than the background surface temperature, cloud is detected.

Surface temperature analyses are available every three hours at AFGWC. Over land areas, surface temperature values are updated once every three hours; over ocean boxes, temperatures are updated once every one or two days.

For the 82162 case study, surface temperature analysis fields over land boxes were available for 18 UTC and 21 UTC. In addition, a three-hour forecasted surface temperature field with a valid time of 00 UTC for day 82163 was available. For the AFGL RDNEPH, a composite surface temperature field was generated for day 82162 by time-interpolating the three-hour temperature values to the actual times of the IR satellite data. Land boxes with satellite overpass times that fell outside the surface temperature analysis times were retained in the composite temperature analysis but were excluded from processing by both analysis algorithms.

All of the temperature data for the water boxes were one to three days older than

the corresponding satellite data. However, since ocean surface temperatures do not change significantly on three-day time scales, all these data were accepted for inclusion into the 82162 hemispheric composite surface temperature field and all of these grid boxes were processed.

A similar composite temperature field was produced for day 85009. However, for this day, five analysis times of surface temperatures were available: 12, 15, 18, and 21 UTC for day 85009, and 00 UTC for day 85010. Since more surface temperatures were available, more satellite data were processed over land boxes for day 85009 than were processed for day 82162. Eighth-mesh processing flags were set up to indicate whether a particular grid box was to be processed (see Section 3.1.2).

Figures 15a and 15c contain displays of the composite hemispheric surface temperature fields used by the AFGL RDNEPH for days 82162 and 85009. Note the seasonal changes between the displays. In addition, Figure 15b contains displays of the five surface temperature fields that were used to generate the composite field for day 85009. Note the diurnal changes from one time to the next.

**Temperature Profiles.** Atmospheric temperature profiles are used in the nephanalysis to compute heights of cloud layers. Having determined the temperature of a given cloud layer from the IR processor, a cloud top altitude is assigned to that layer using the temperature-height profiles. Temperature profiles are at whole-mesh resolution and are normally updated from two to four times daily. Temperatures and heights are given at ten standard pressure levels: 1000, 850, 700, 500, 400, 300, 250, 200, 150, and 100 mb.

### 3.1.2 EIGHTH-MESH PROCESSING FLAGS

The satellite data used for the two case studies in this comparison investigation consist of a "snapshot" of the SGDB, that is, the SGDB is frozen at one instant in time and saved. Since the SGDB is a dynamic data base, with new data constantly being added, the snapshot necessarily contains satellite data of varying ages. As described in Section 3.1.1, surface temperature data were obtained from AFGWC for a number of different time periods preceding the valid time of the SGDB. To insure that the supporting data (most notably the surface temperatures) match the satellite data temporally at each quarter-mesh box, stringent timeliness checks are made among the various data sources. The timeliness check requires that for land boxes to be processed, the valid time of the satellite data at each quarter-mesh box must fall within the times for which surface temperature analyses are available. When this condition is met, the surface temperature values that bracket the satellite time are interpolated to the satellite time and stored in the composite eighth-mesh surface temperature data file. A separate field of processing flags is maintained concurrently for each eighth-mesh grid point. These flags are set when timely surface temperature data is available for a given eighth-mesh point. The timeliness criterion is relaxed for

ocean surfaces. Ocean surface temperature analyses of up to 72 hours prior to the satellite valid time are accepted.

After the surface temperature data are analyzed for timeliness and subsequently interpolated, the background brightness data are checked for a match with the satellite ID in the SGDB. If there are no background brightness data available that match the satellite ID of a quarter-mesh box, all eighth-mesh processing flags within the quarter-mesh box are cleared. The processing flags are checked during the cloud analysis, and an eighth-mesh box is not processed if the flag is not set. The eighth-mesh processing flag database is used only by the AFGL RDNEPH. Figures 16 and 18 contain hemispheric displays of the SGDB that show IR grayshades where the eighth-mesh flags are set, and black where the flags are not set.

#### **4. COMPARISON RESULTS**

The comparison study of the RTNEPH and AFGL cloud layer algorithms was performed using the hemispheric case study data described in Section 3. The two algorithms under investigation were run on the data for both days using the RDNEPH program to insure consistency. RDNEPH output provides detailed information on cloud amount, cloud layer distribution, and cloud height for each analysis box in the hemisphere. This information was used to compute summary statistics for the different analyses. In turn the statistics were used to characterize the differences between the two analysis algorithms.

In this section, the RDNEPH products that were used in the comparison analysis are described. In addition the various statistics that were used for characterizing the algorithm results are introduced. Results of the RDNEPH runs are presented for each algorithm/case study combination.

##### **4.1 Representative Grayshade Images**

Representative grayshade (RGS) images are synthetic images that pictorially represent the cloud analysis of the IR processor. They are used extensively at AFGL to evaluate visually the automated RDNEPH cloud analyses. RGS images are constructed by doing a pixel-by-pixel replacement of the original SGDB IR image with a representation of the cloud layer and height analyses that corresponds to that IR image. As such, RGS images retain the same spatial distribution of cloud and background features contained in the original IR image. This is an important attribute of the RGS display since the eye relies on recognition of spatial patterns to interpret an image.

The value of an RGS pixel is determined through a series of tests. If an IR pixel is analyzed by the cloud algorithm as clear, the RGS is assigned a reserved value that

represents the background type at that location (obtained from the geography data base). If the IR pixel is cloudy, the RGS is assigned an intensity value that corresponds to the analyzed cloud layer temperature. The intensity value is obtained from the same grayshade-to-temperature lookup table used by the RDNEPH to obtain IR brightness temperatures from the SGDB data. In this way cloudy portions of the RGS image retain an appearance similar to the original IR image.

Once all the grayshades are assigned to the RGS image, the clear pixels are color-enhanced to facilitate the easy identification of the backgrounds. RGS water pixels are colored light blue; land pixels dark green; ice pixels dark blue; and coastlines bright green. The cloudy RGS pixels are enhanced in shades of gray. The brighter the cloudy RGS pixel, the higher the cloud layer. Note that each cloud layer within a given eighth-mesh box has its own unique RGS grayshade. Thus, when an RGS image is examined, clear regions (in color) stand out sharply against cloudy regions (in shades of gray). In addition, multiple cloud layers are distinguishable as differing shades of gray. Table 2 lists the values for RGS grayshades. An example of a hemispheric RGS image for day 82162 is shown in Figure 17; for 85009, see Figure 19.

By displaying the RTNEPH or AFGL cloud analyses as RGS images, cloud layer details are seen on a scale that is as fine as the input satellite data. RGS images allow for a direct, one-to-one comparison between the SGDB imagery and the RDNEPH cloud analysis output. Compare the RGS images in Figures 17 and 19 with the SGDB images in Figures 16 and 18, respectively. This type of visual comparison is useful for evaluating the accuracy and the characteristics of the NEPH output. Many important features that are lost in the coarser eighth-mesh cloud analysis are clearly noticeable within the sixty-fourth-mesh RGS image.

## 4.2 RDNEPH Statistics

Summary statistics of the RDNEPH output data are computed and displayed in tabular and/or graphical form. These statistical calculations use as input the cloud analysis data produced by the RTNEPH and AFGL algorithms. The RDNEPH statistics help quantify the differences between the two cluster algorithms and, if desired, between the algorithms and ground truth. Statistics can be computed for a complete hemispheric analysis, for specific RTNEPH boxes, for particular geography types (for example, land/coast vs. water/ice), for a specified atmospheric layer (for example, low, middle, or high), or even for a specific time of day. The following is a description of the statistics that are generated for an RDNEPH cloud analysis and how those statistics are derived.

<b>RGS Grayshade Values For Clear Pixels</b>		
<i>RGS Value</i>	<i>Geography Type</i>	<i>Color Enhancement</i>
0	Off-Hemisphere	Black
1	Water	Light Blue
2	Land	Dark Green
3	Ice	Dark Blue
4	Coastline	Bright Green
≥4	Clouds	Grayshades

**Table 2.** Representative Grayshade Values for Clear and Cloudy Pixels

**Layer Cloud Amount.** The average cloud amount per layer "n" (where n ranges from 1 to 4) is computed by summing the percent coverage of each cloudy layer that has at least 1 percent cloud, and dividing by the number of times that layer occurs within an eighth-mesh box. This calculation can be done only for RDNEPH cloud analyses and not for cloud truth since layer information is not yet provided as a part of the cloud truth database (see Section 4.3). Figure 2 contains examples of plots of cloud amount vs. layer number for the RTNEPH and AFGL algorithms for the 1982 and 1985 case study days.

**Layer Frequency Distributions.** Layer frequency distributions are built by counting the number of times layer "n" occurs within all processed eighth-mesh boxes. The RTNEPH and AFGL algorithms allow up to a maximum of four layers. The average number of cloud layers per eighth-mesh box is also computed as a routine part of the statistics calculations.

Figure 3 contains plots of the number of eighth-mesh boxes vs. number of layers for the RTNEPH and AFGL algorithms for day 82162. Note that the AFGL algorithm tends to find fewer layers than the RTNEPH algorithm.

**Distribution of Total Cloud Amount Per Eighth-mesh Box.** Determination of the frequency distribution of cloud amount per eighth-mesh grid box is also a part of the statistics calculations. The cloud amount distribution through either a specified layer or throughout the entire depth of the atmosphere can be computed. When cloud amount distributions for a layer are computed, the total layer cloud amount is computed by adding together the cloud amount for each cloud that has a top within that layer. Using such a scheme, it is possible to have layer cloud amounts greater than 100 percent due to layer-averaging and roundoff procedures that are a part of the RTNEPH.

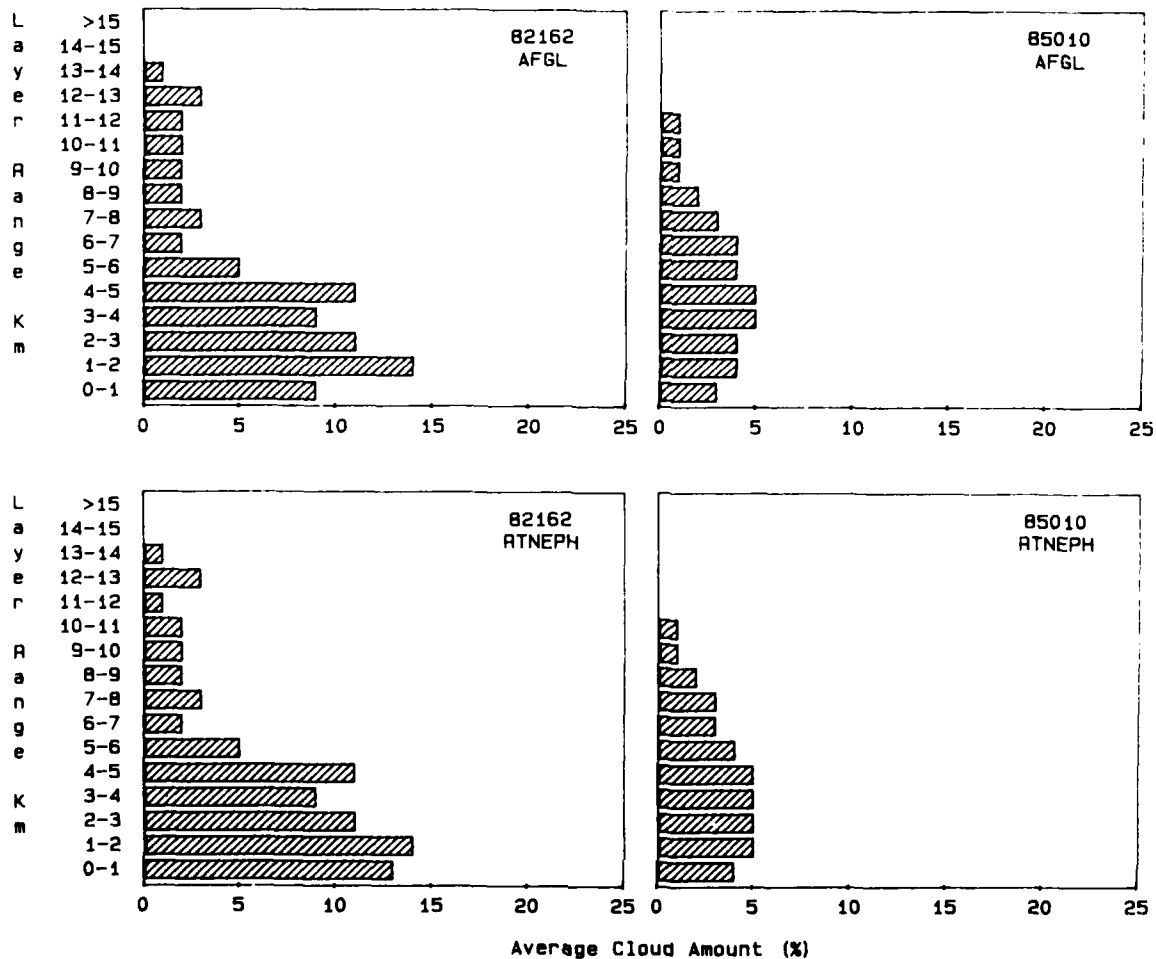
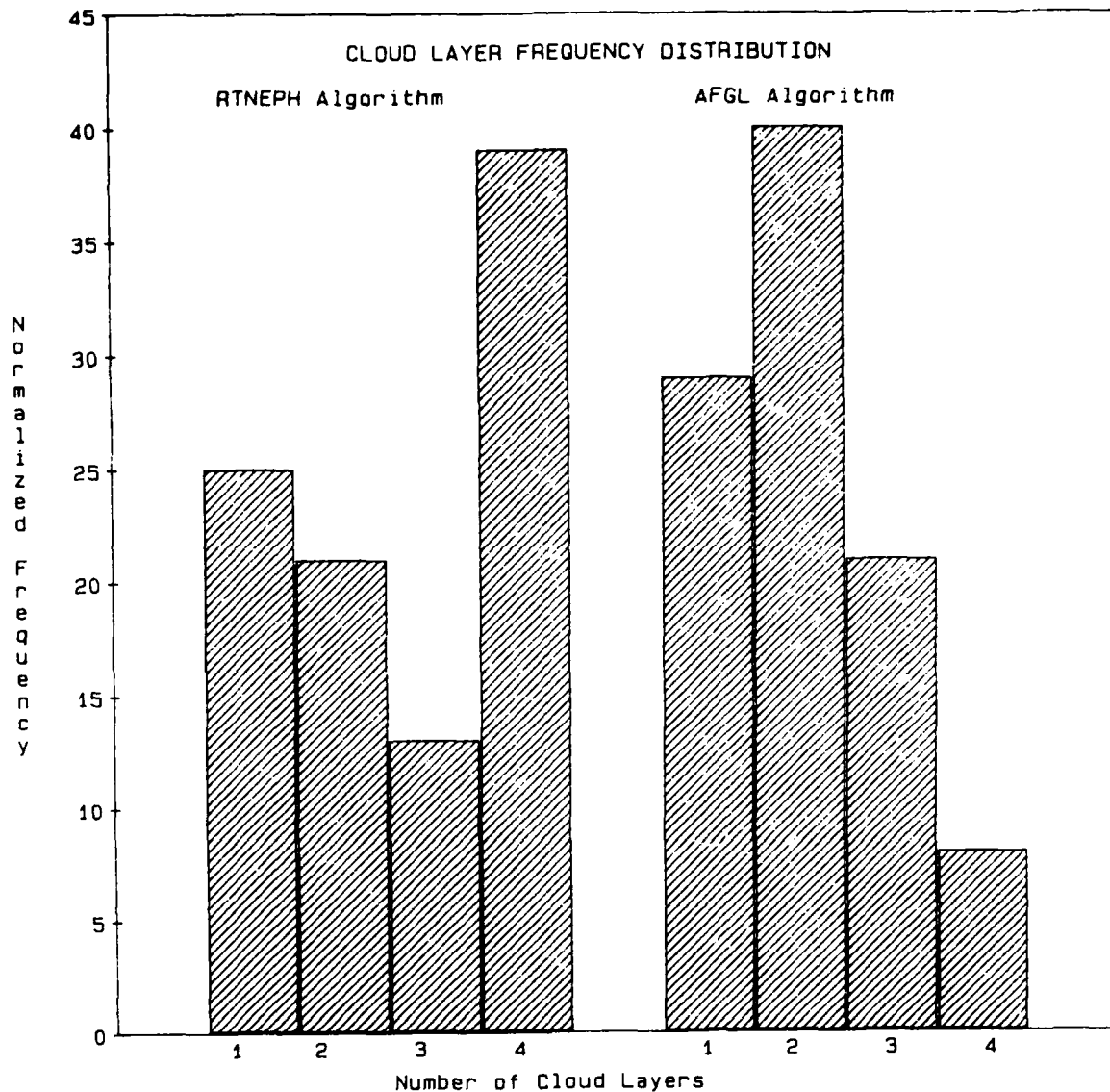


Figure 2. Plot of Average Cloud Amount Per Layer for the RTNEPH and AFGL Algorithms

Cloud amount distributions can be stratified in several different ways. For example, they can be computed for a limited set of RTNEPH boxes (for example, all land or all water boxes) or for a range of latitudes (for example, for the tropics, mid-latitudes, or polar regions). Figure 4 shows the distribution of eighth-mesh boxes as a function of total cloud amount for the full hemisphere, day 82162. Note the high number of boxes that are either completely clear or cloudy.

**Cloud Amount As a Function of Viewing Angle.** Cloud amount vs. viewing angle curves are computed by mapping the analyzed total cloud amount to the satellite viewing angle for an eighth-mesh box. When the curves are generated from nephanalyses that cover large regions of the globe or that cover long periods of time, they show biases in cloud amount as satellite viewing angles change. Typically, cloud amounts increase as viewing angle increases due to infrared atmospheric attenuation



**Figure 3.** Sample Plot of Frequency Distribution of Number of Layers for the RTNEPH and AFGL Algorithms

and cloud geometry considerations. Atmospheric attenuation causes a given scene to appear colder, and hence potentially more cloudy, at higher viewing angles. The geometrical shapes of clouds dictate that as viewing angles increase, less of the tops and progressively more of the sides of clouds are viewed by a satellite sensor. For clouds with large vertical extents in partially cloudy scenes, the potential exists for seeing, and subsequently confusing, more of the sides of clouds. This can translate to an increase in analyzed cloud cover even though the actual earth cover remains unchanged. Figure 5 plots how cloud cover varies with viewing angle for the case study day 82162. Note the tendency for cloud amount to increase at larger viewing angles.

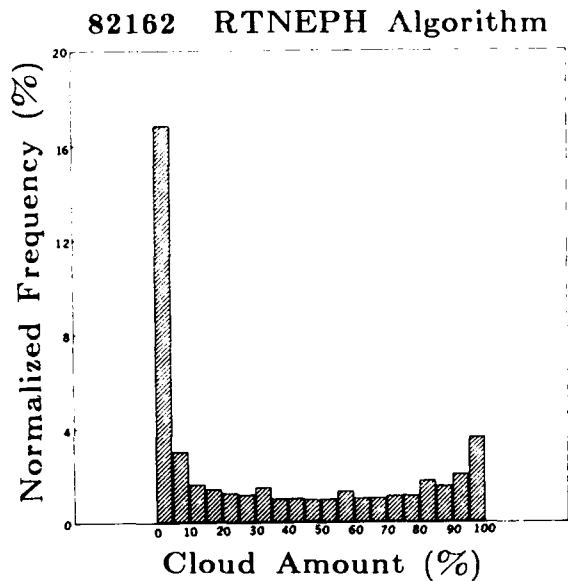


**Figure 4.** Sample Plot of the Frequency Distribution of Total Cloud Amount

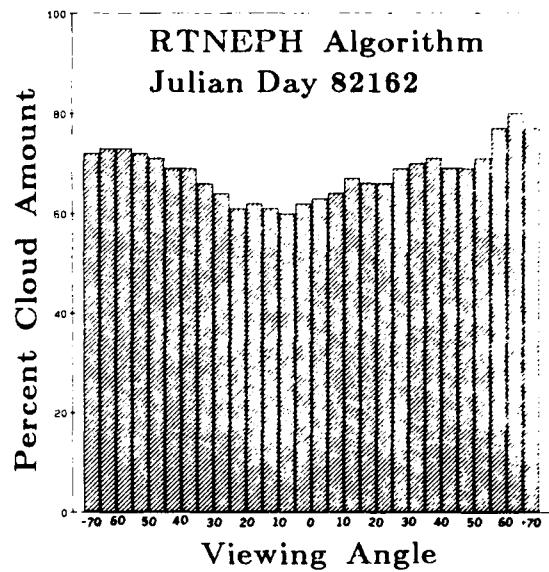


**Figure 5.** Sample Plot of Total Cloud Amount vs. Viewing Angle

**Cloud Height.** The average cloud height within a specified atmospheric layer is computed. These statistics illustrate a key difference between the characteristics of the AFGWC and AFGL cloud layer analyses. This topic is discussed in more detail in Section 5.

**Sharpness.** Sharpness is the percentage of eighth-mesh boxes that have total cloud amounts in either the 0 - 20 percent range (nominally clear) or the 80 - 100 percent range (nominally overcast). Sharpness values for both the 82162 and 85009 case study days are approximately 85 percent (see Figure 4).

### 4.3 Cloud Truth Images

Quantitative evaluation of the accuracy of cloud detection algorithms can be problematic due to the general lack of cloud ground truth. Even surface-based cloud observations are difficult to use because of the radically different viewing geometries of a surface observer and a satellite. In an effort to make some type of quantitative estimate of the cloud detection accuracy of the two algorithms under investigation here, manual cloud analyses were made for selected RTNEPH boxes for use as ground truth. The manual analyses were generated from the same SGDB visible and infrared data used by the automated algorithms. To aid image interpretation, the full range of image processing and display functions of the AIMS imaging computer system were used.

The procedure for generating manual cloud analyses on AIMS is a well defined iterative procedure designed to produce an optimal analysis given the quality of the data (see Gustafson and Felde, 1988; 1989). First, both the infrared and visible



imagery for a selected RTNEPH box are displayed. The analyst selects a subregion of the box for analysis. The data from one or both of the satellite channels for the selected subregion are isolated and loaded onto a clear screen on the display device. Different interactive contrast enhancements and display options can be applied to the imagery to help the analyst identify the cloud boundaries. Cloud boundary location is then transferred into a digital file in the computer through a process known as threshold blanking. Threshold blanking is an interactive technique that allows for very accurate selection, isolation and extraction of cloud features that the analyst has identified visually. The procedure is repeated for different sub-regions of the RTNEPH box until the analyst is satisfied that all cloud boundaries have been accurately identified. The manual analysis is stored as a synthetic binary image that can be directly compared to the automated analysis. At AFGL these synthetic images are referred to as cloud truth. Statistical evaluations of the agreement between the automated analyses and cloud truth can be used to provide a quantitative measure of the cloud detection accuracy.

Midway through the term of this comparison study a change, known commonly as the sharpness fix, was made in the RTNEPH cloud detection procedure at AFGWC. Recall from Section 2.1.2 that the RTNEPH layer analysis combines pixels of an  $8 \times 8$  IR array into thermally homogeneous clusters. Before the sharpness fix was incorporated into the RTNEPH, the cloud layer analysis would be performed on the complete IR array, even though the pixels often represent a mix of clear and cloudy scenes. The clear/cloud decisions were then made on a cluster-by-cluster basis, rather than on a pixel-by-pixel basis. This offered the potential for misinterpreting some pixels depending on how well the algorithm segregated clear and cloudy pixels into separate clusters. For example, if a cluster contains both clear and cloudy pixels, then an error in total cloud amount would always be incurred by the RTNEPH because that cluster is flagged as either completely clear or completely cloudy. Hence differences in the way each algorithm performed the cluster separations resulted in differences between the total cloud amounts detected by the RTNEPH and AFGL algorithms.

However, the sharpness fix reversed the order of processing, so that the clear/cloud decision is now made prior to the layer analysis (refer to paragraph 1 of Section 2.1.2). This means that all clear pixels are removed from consideration before being processed by the layer algorithm. As expected, sharpness was smaller in every instance (that is, with the sharpness fix) by an average of 6 percent.

Before comparing the RTNEPH and AFGL layer analyses, the sharpness fix was incorporated into both programs. One of the consequences of this fix is that the differences between the ways the RTNEPH and AFGL cloud algorithms perform cloud detection are eliminated. As a result, the total cloud amounts computed by each algorithm are equal, although significant differences remain in the cloud layer results. After the changes were implemented in the AFGL test programs, cloud

detection accuracy was removed as a comparison criteria as far as this study is concerned. However, it is still of interest to compare analyzed cloud amounts with cloud truth images to determine how accurate the automated analysis is.

Figure 6a shows an RGS image (see Section 4.1) for RTNEPH Box 45 taken from the 82162 case study. The corresponding visible and infrared satellite data are shown for reference in Figures 6c and 6d. Figure 6b contains a truth image which is interpreted in the same way as the RGS; color-enhanced pixels represent clear regions while cloudy areas are in shades of gray. By comparing RGS and truth images it is easier to visualize how the RTNEPH and the AFGL algorithms perform relative to truth and relative to each other. Although not required of this study, such comparisons will be useful in future nephanalysis studies that deal with viewing angle bias and the improved detection of low clouds and thin cirrus.



**Figure 6a.** RGS Cloud Analysis Image for RTNEPH Box 45, Summer Day 82162. Color-enhanced pixels denote clear regions, and gray pixels denote clouds



**Figure 6b.** Cloud Truth Image for RTNEPH Box 45, Summer Day 82162. Color-enhanced pixels denote clear regions, and gray pixels denote clouds

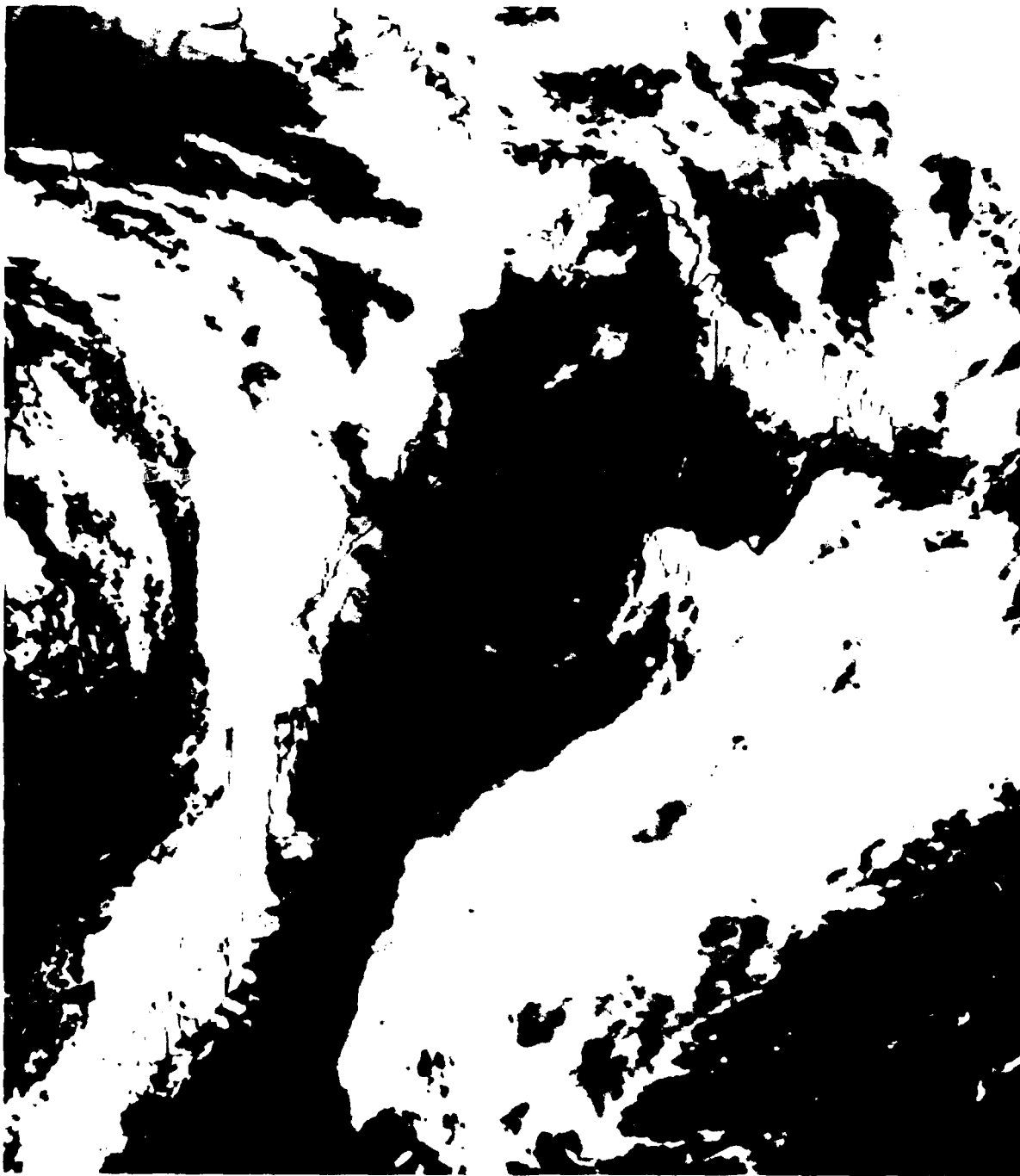


**Figure 6c.** Visible Image for RTNEPH Box 45, Summer Day 82162. Bright tones denote high solar reflectance; dark tones denote low reflectance

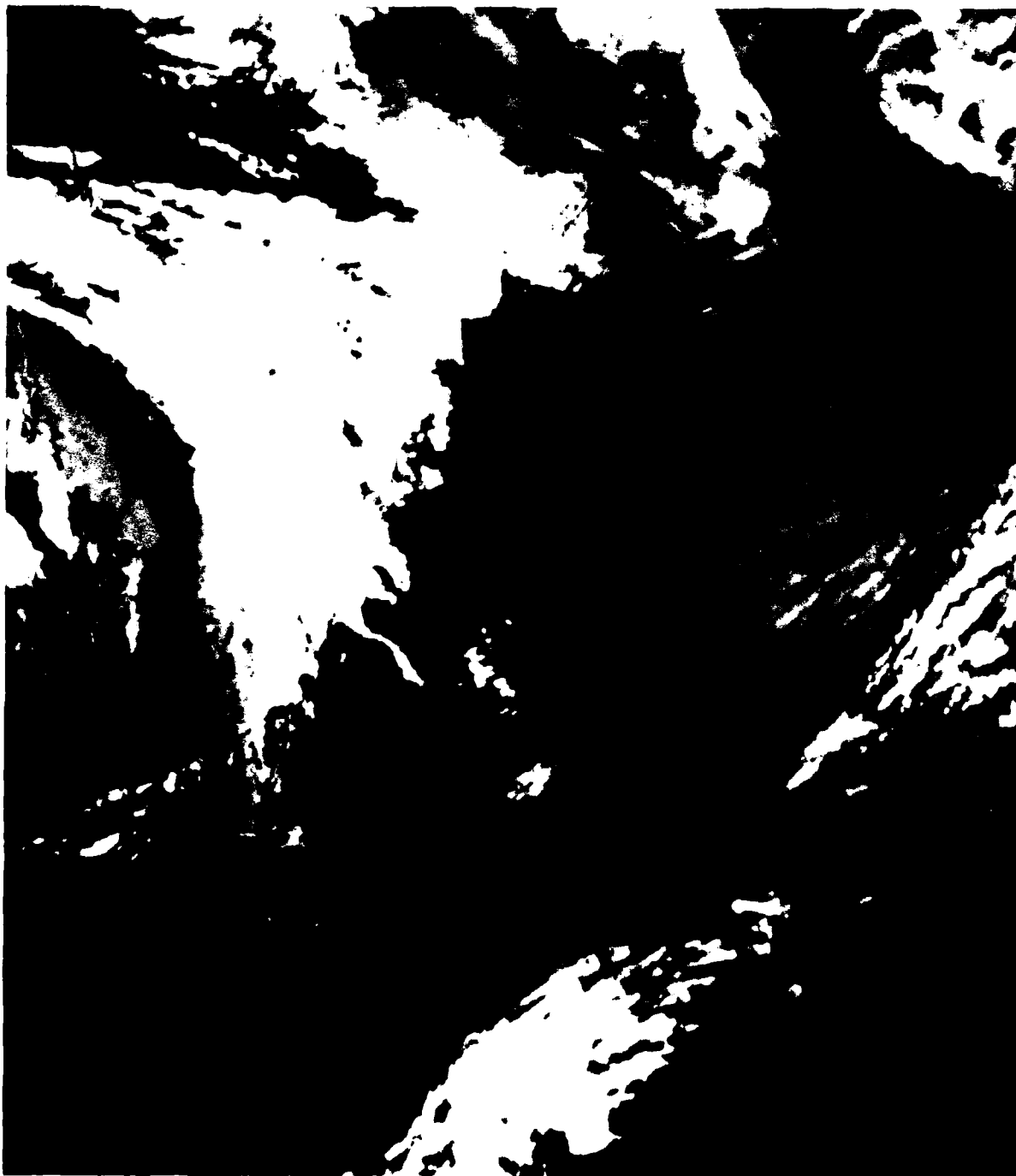


**Figure 6d.** Infrared Image for RTNEPH Box 45, Summer Day 82162. Bright tones denote low brightness temperatures; dark tones denote high temperatures

## 5. DISCUSSION

The results of the RTNEPH and AFGL layer analyses are presented in the following sections. The layer analyses are not precisely as they would be in the operational AFGWC RTNEPH cloud analysis because merge processing of the cloud data has been excluded; that is, the results presented here were generated by the IR processor only. However, these results allow for interesting and valuable comparisons between the AFGL and RTNEPH layer algorithms, and highlight characteristic differences between the two that would be observed if each were a merged nephanalysis.

### 5.1 Cloud Layers

Tables 3 and 4 summarize the nephanalysis cloud layer statistics by background type and algorithm. The data in Table 3 for summer show higher cloud amounts and more cloud layers for both algorithms than the data shown for winter in Table 4. The statistics also indicate a consistently different distribution of layer frequencies for the RTNEPH and AFGL algorithms. The column headed "Layer Frequency (percent)" gives the distribution of the number of layers found per eighth-mesh box. For the RTNEPH algorithm, Table 3 shows for land/coast backgrounds that 13 percent of the time, one cloud layer was found in an eighth-mesh box; 20 percent of the time, two were found; 15 percent of the time, three were found; and 50% of the time, four were found. (The percentages do not usually sum to 100 since they are truncated to whole numbers when they are computed.) Note that four cloud layers are found by the RTNEPH algorithm more frequently than three cloud layers. All of the other RTNEPH layer frequencies in Tables 3 and 4 share this unusual distribution, with lower frequencies of three cloud layers than of either four or two. There is no apparent explanation for this distribution either in the logic of the RTNEPH algorithm or in the literature of cloud observations.

The AFGL algorithm, on the other hand, has a layer frequency distribution that is consistently smoother than that of the RTNEPH algorithm, as can be seen in Tables 3 and 4. The AFGL distribution has a peak frequency for two cloud layers in summer (Table 3) and for one cloud layer in winter (Table 4). The frequencies decrease for three and four cloud layers.

The difference in the RTNEPH and AFGL layer frequency distributions are also shown in the plots of Figure 7 for the summer and winter cases. There is a substantial difference in the number of times that the RTNEPH and AFGL algorithms find four cloud layers — 38 percent compared to 8 percent for summer, and 18 percent compared to 2 percent for winter. The higher frequency of four cloud layers in the RTNEPH contributes to a higher average number of layers per eighth-mesh box; 2.10 for AFGL compared to 2.69 for RTNEPH in summer, a 28 percent increase; and 1.64 for AFGL compared to 1.97 for RTNEPH in winter, a 20 percent

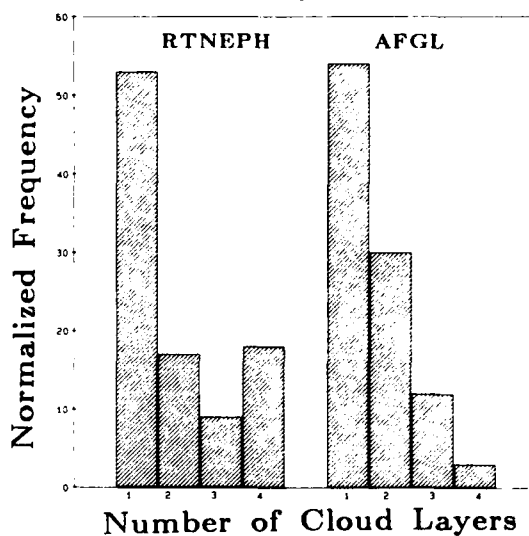
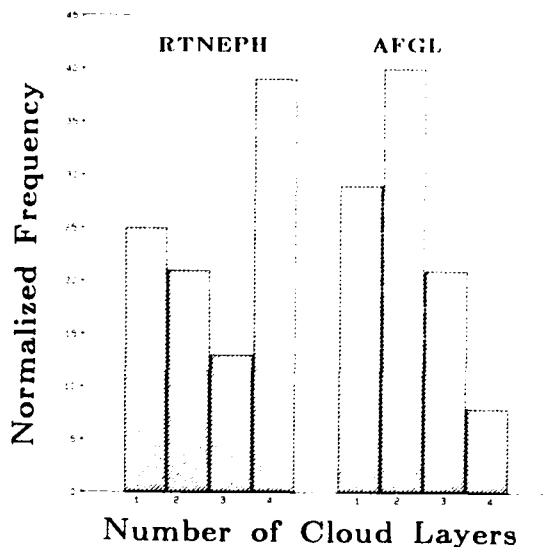
Nephanalysis Infrared Processor Hemispheric Statistics — Summer — Day 82162								
Cloud Top Height Range: Total ( 0 — 22500 m )								
Background (# 1/8th-Mesh Boxes Processed)	Algorithm	Layer Frequency (%)				Ave. # of Layers Per 1/8 Box	Average Cloud Amount (%)	Average Cloud Height (m)
		1	2	3	4			
Land/Coast (26622)	RTNEPH	13	20	15	50	3.09	81	4604
	AFGL	15	44	29	10	2.37	81	4856
Water/Ice (123502)	RTNEPH	28	22	12	36	2.60	67	4154
	AFGL	32	39	19	7	2.04	67	4398
All Types (150124)	RTNEPH	25	21	13	38	2.69	70	4252
	AFGL	29	40	21	8	2.10	70	4498

Table 3. IR Processor Hemispheric Statistics for the Summer Case Study Day 82162



Nephanalysis Infrared Processor Hemispheric Statistics — Winter — Day 85009								
Cloud Top Height Range: Total ( 0 — 22500 m )								
Background (# 1/8th-Mesh Boxes Processed)	Algorithm	Layer Frequency (%)				Ave. # of Layers Per 1/8 Box	Average Cloud Amount (%)	Average Cloud Height (m)
		1	2	3	4			
Land/Coast (64973)	RTNEPH	64	15	7	11	1.71	23	4832
	AFGL	64	24	8	2	1.48	23	5166
Water/Ice (116457)	RTNEPH	47	19	10	21	2.12	38	3992
	AFGL	48	34	14	3	1.73	38	4408
All Types (181430)	RTNEPH	53	17	9	18	1.97	33	4206
	AFGL	54	30	12	2	1.64	33	4605

Table 4. IR Processor Hemispheric Statistics for the Winter Case Study Day 85009



**Figure 7.** Plots of Layer Frequency as a Function of the Number of Cloud Layers for the RTNEPH and AFGL Algorithms (See Tables 3 and 4 - Layer Frequency Statistics)

increase. RTNEPH tends to find more cloud layers than AFGL. This results in a significantly cloudier RTNEPH because of the upper cloud occlusion algorithm that is a part of the merge processor. The cloud occlusion algorithm increases the lower-layer cloud amounts by 5 - 10 percent for each layer, which would cause significant differences between the final cloud analyses of the RTNEPH and AFGL algorithms.

Tables 3 and 4 cover all cloud top heights. Tables 7 - 12 were generated for the low (0 - 2000 m), middle (2001 - 6000 m), and high (6001 - 22500 m) ranges of cloud top height (see Section 8). Within each range, the RTNEPH algorithm finds small frequencies of occurrence (5 - 10 percent) of three or four cloud layers, while the AFGL algorithm rarely finds more than two. The average number of cloud layers within each range of cloud heights is consistently greater for the RTNEPH algorithm. These results suggest that the tendency of the RTNEPH algorithm to find more cloud layers than the AFGL algorithm is independent of cloud altitude and does not favor any cloud type.

Comparison of the layer frequency distributions between the RTNEPH and AFGL algorithms reveal essentially the same results as the earlier comparison study between the 3DNEPH and AFGL algorithms (d'Entremont et al., 1982). In that study both algorithms had a tendency to find more cloud layers than were identified by satellite meteorologists who made a subjective assessment of infrared and visual pictures supplemented by surface reports. Assessments of the pictures rarely indicated the presence of three or four cloudy layers. The AFGL algorithm was preferred since it was less likely to overestimate the number cloud layers. It is

preferred now for the same reason.

## 5.2 Cloud Heights

Average cloud heights are given in the last column of Tables 3 and 4. For the summer case study day (Table 3) over all types of backgrounds, the RTNEPH gives an average cloud height of 4252 meters, which is 246 meters less than the average cloud height found by the AFGL algorithm. For the winter day (Table 4), the RTNEPH average height is 4206 meters, which is 399 meters less than the AFGL algorithm. The average difference between the RTNEPH and AFGL cloud heights is equivalent to roughly one infrared grayshade value. This is because one grayshade represents a temperature range of 1.9 K and atmospheric temperatures decrease by this amount when altitudes increase by 300 meters, excepting inversions.

From summer to winter, changes in average cloud heights for the RTNEPH algorithm are on the order of 50 m; the same is true for the AFGL algorithm. The 50 m change is surprisingly small, considering that tropopause heights and cirrus cloud heights tend to be 1 - 2 km lower in the winter over much of the hemisphere. The explanation is that the winter case had fewer low clouds than the summer case as can be seen in Figures 8 to 11.

Figures 8 to 11 show the height distribution of average cloud amount and number of layers for the five layers of 5LAYER, the main cloud forecast model at AFGWC (Crum, 1987). The 5LAYER produces cloud forecasts at the gradient level and the 850, 700, 500 and 300 mb levels. The altitude ranges for each of these layers are listed in Table 5.

Figures 8 and 9 show the RTNEPH and AFGL results for the summer case. Results are stratified by latitude into tropical, mid-latitude, and polar regions. The latitude bounds for these regions change seasonally; the bounds for the summer and winter case study days are the same as those used by the RTNEPH, and are listed in Table 6. The lower set of bar graphs in Figure 8 shows how all the cloud tops found by the RTNEPH are distributed among the 5LAYER layers. For example, the mid-latitude graph shows that 35 percent of the cloud tops found by the RTNEPH fall within the 700 mb layer. The upper set of bar graphs in Figure 8 plots average cloud amounts per layer. These are computed by summing the observed cloud percentages within the five defined layers and dividing by the total number of eighth-mesh boxes for the latitude band. For mid-latitudes, the average cloud amount in the 700 mb layer is 25 percent.

The distributions of average cloud amount in Figures 8 (for the RTNEPH algorithm) and 9 (for AFGL) are unusual in two respects. The 500 and 300 mb layers include an altitude range suitable for nearly all cirrus clouds at all latitudes, but have significantly lower cloud amounts than published climatologies using surface or satellite observations would indicate (Hall et al., 1984; Izumi, 1982; Hahn et al.,

<i>5LAYER Layer #</i>	<i>Centroid Pressure</i>	<i>Height Range (meters)</i>
1	"Gradient"	0 - 987
2	850 mb	988 - 2235
3	700 mb	2236 - 4239
4	500 mb	4240 - 7369
5	300 mb	7370 - 22500

**Table 5.** Altitude Ranges for the Layers of the 5LAYER Cloud Forecast Model

<i>Region</i>	<i>Season</i>	<i>Latitude Bounds</i>
Tropics	Summer	0° - 29.9°
	Winter	0° - 23.5°
Mid-Latitude	Summer	29.9° - 72.9°
	Winter	23.5° - 66.5°
Polar	Summer	72.9° - 90.0°
	Winter	66.5° - 90.0°

**Table 6.** Latitude Bounds for the Tropics, Mid-latitudes, and Polar Regions for the Summer and Winter Case Study Days

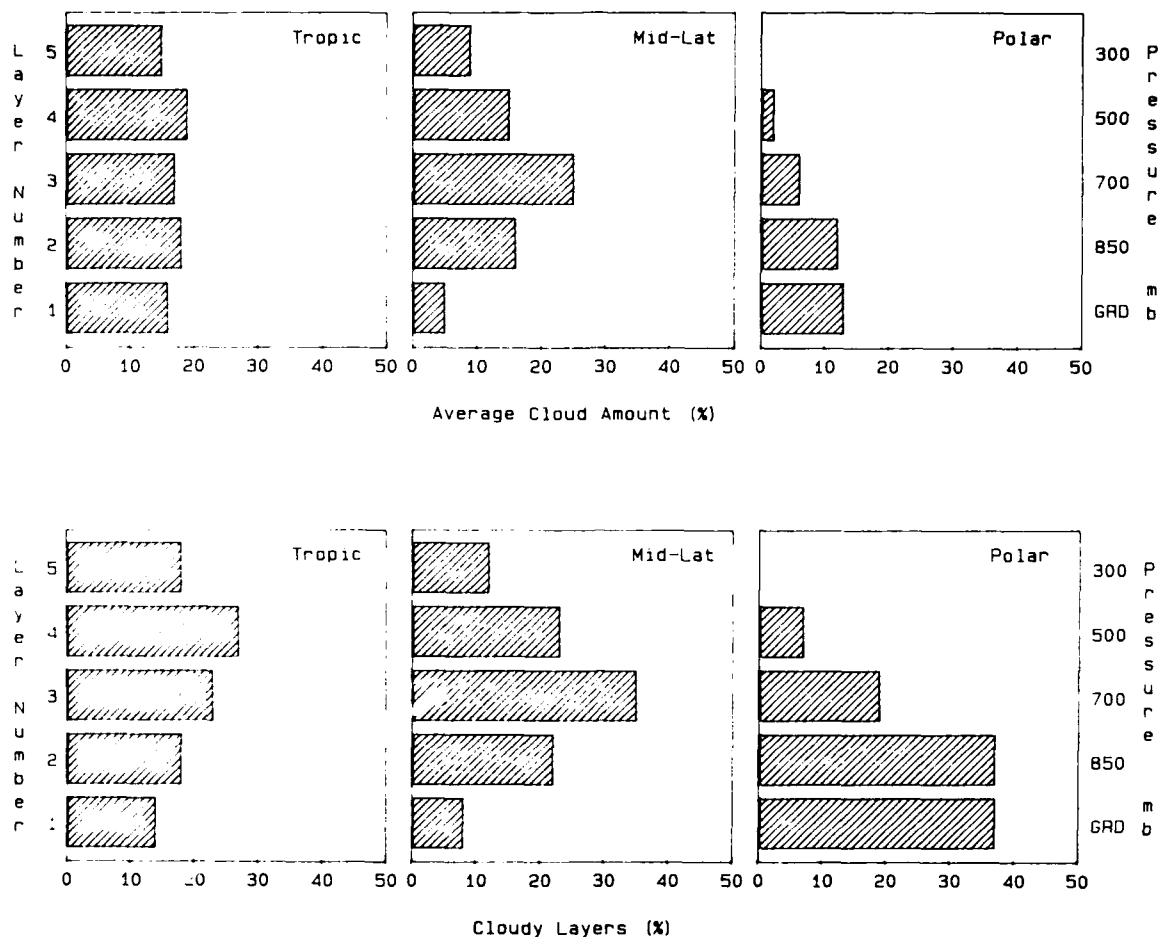


**Figure 8.** Plots of Hemispheric Cloud Layer Distributions and Average Layer Cloud Amounts as a Function of Height for the RTNEPH Algorithm, Summer Day 82162 (See Table 13)

1982; Woodbury and McCormick, 1983). These sources give cirrus frequencies of occurrence that range from 30 percent to 60 percent (when sub-visual cirrus was included) for mid-latitude and sub-polar regions during the summer. The cloud amount in the 300 mb layer is only 9 percent for the RTNEPH mid-latitude summer, yet the altitude range of that layer should include most cirrus clouds in the mid-latitude summer. The AFGL algorithm (Fig. 9) found 10 percent for the mid-latitude summer. We attribute the small cloud amounts found in the 300 mb layer to optically thin cirrus that appears warmer to the infrared sensor than the ambient atmospheric temperature at cirrus altitudes. These clouds tend to be assigned lower altitudes by the IR satellite processor. In Figures 8 and 9 it is seen that the average cloud amounts in the 300 mb layer change as expected in going from the tropics to polar regions, since the amount of high clouds consistently decreases with latitude as the tropopause lowers.

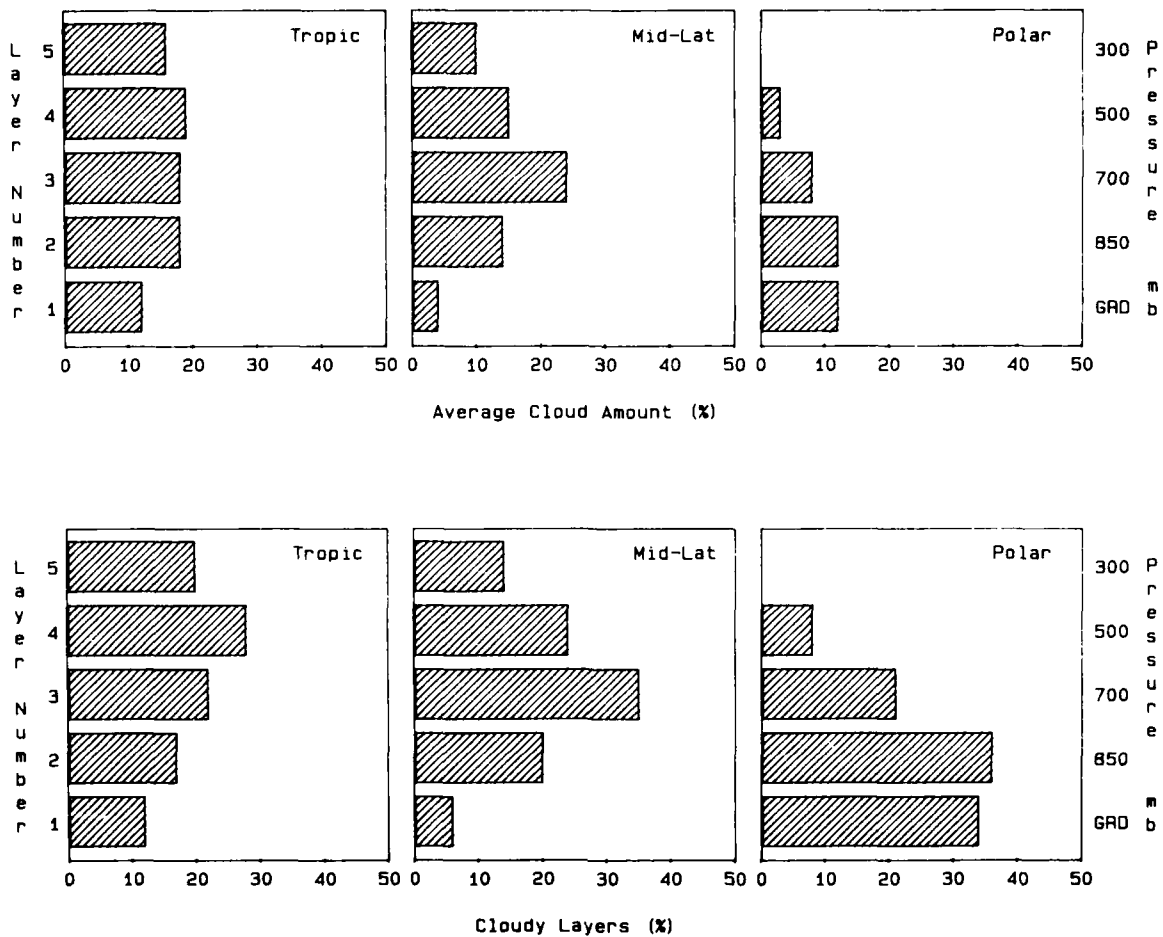


**Figure 9.** Plots of Hemispheric Cloud Layer Distributions and Average Layer Cloud Amounts as a Function of Height for the AFGL Algorithm, Summer Day 82162 (See Table 14)

The other unusual aspect of Figures 8 and 9 is the peak in average cloud amount for the 700 mb layer in the mid-latitudes. Higher cloud amounts would be expected in the two lowest layers (deBary and Moller, 1963) or in the cirrus layer, but not in the middle layer. One possible explanation is that the average cloud amount for the middle layer is enhanced by cirrus clouds assigned to the wrong layer.

The most remarkable feature of Figures 8 and 9 is how little difference there is between the RTNEPH and AFGL algorithms when the cloud tops are grouped into the 5LAYER layers. For the 500 and 300 mb layers the AFGL algorithm found cloud amounts that are within 4 percent of the corresponding RTNEPH cloud amounts. The greatest difference between the algorithms is found in the gradient layer of the tropics where the cloud amount decreases from 16 percent for RTNEPH to 12 percent for AFGL. In other latitudes, the RTNEPH algorithm has gradient layer cloud amounts 1 percent greater than the AFGL algorithm.

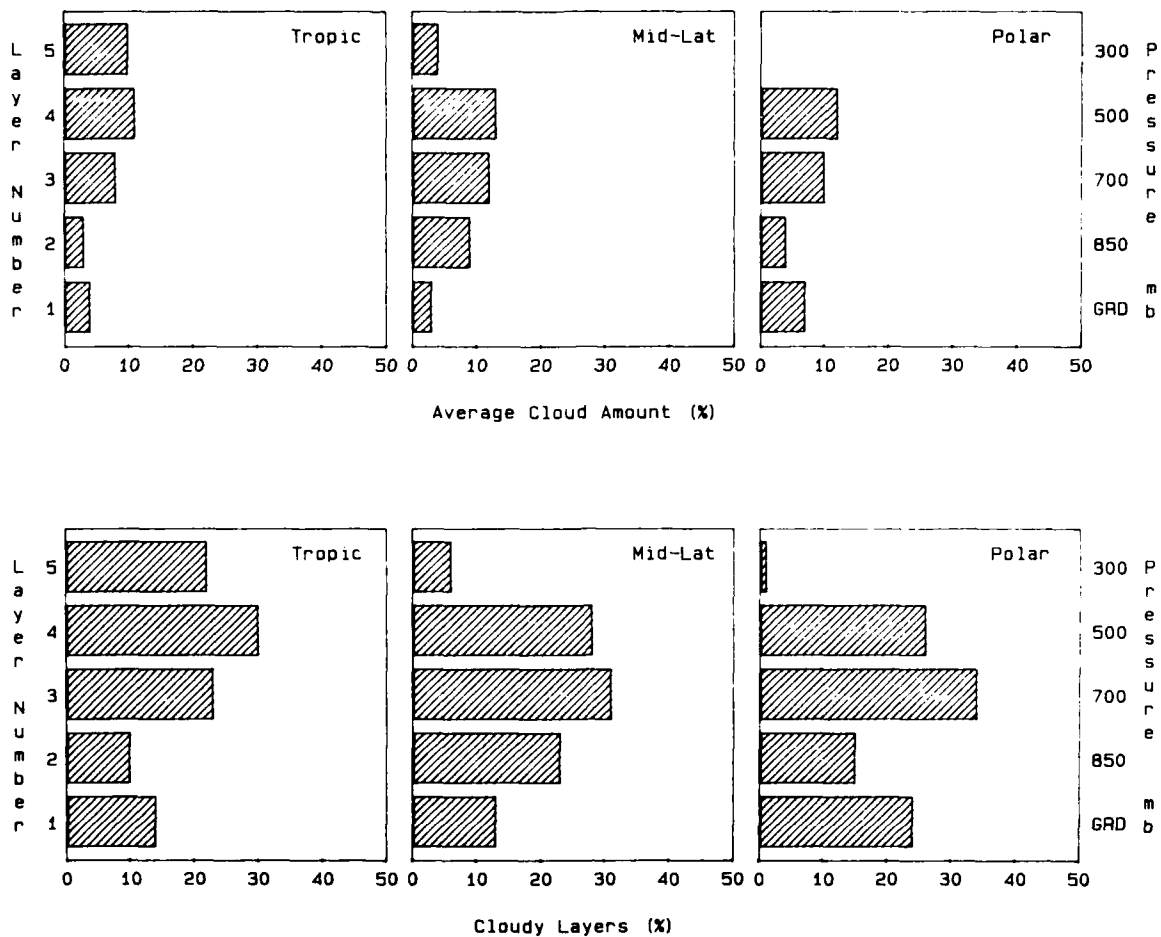


**Figure 10.** Plots of Hemispheric Cloud Layer Distributions and Average Layer Cloud Amounts as a Function of Height for the RTNEPH Algorithm, Winter Day 85009 (See Table 15)

The distribution of cloudy layers shown in the lower parts of Figures 8 and 9 are also nearly identical for the RTNEPH and AFGL algorithms, even though the RTNEPH algorithm found significantly more layers. For example, RTNEPH found a total of 251,333 layers in the tropics while AFGL found only 186,403. However, both algorithms have nearly the same distribution of cloud layers as a function of height. This means the excess cloud layers found by the RTNEPH algorithm must be proportionally distributed among the five layers.

Figures 10 and 11 show the results for the winter case. The cloud layer distributions are rather uniform except for the 300 mb mid-latitude and polar layers. The average cloud amounts are less than the summer values in every instance except for the 700 and 500 mb layers at polar latitudes. As in the summer, the cloud amount averages in the 500 and 300 mb layers are lower than climatological averages of cirrus clouds and the same explanation (optically-thin cirrus) likely applies.

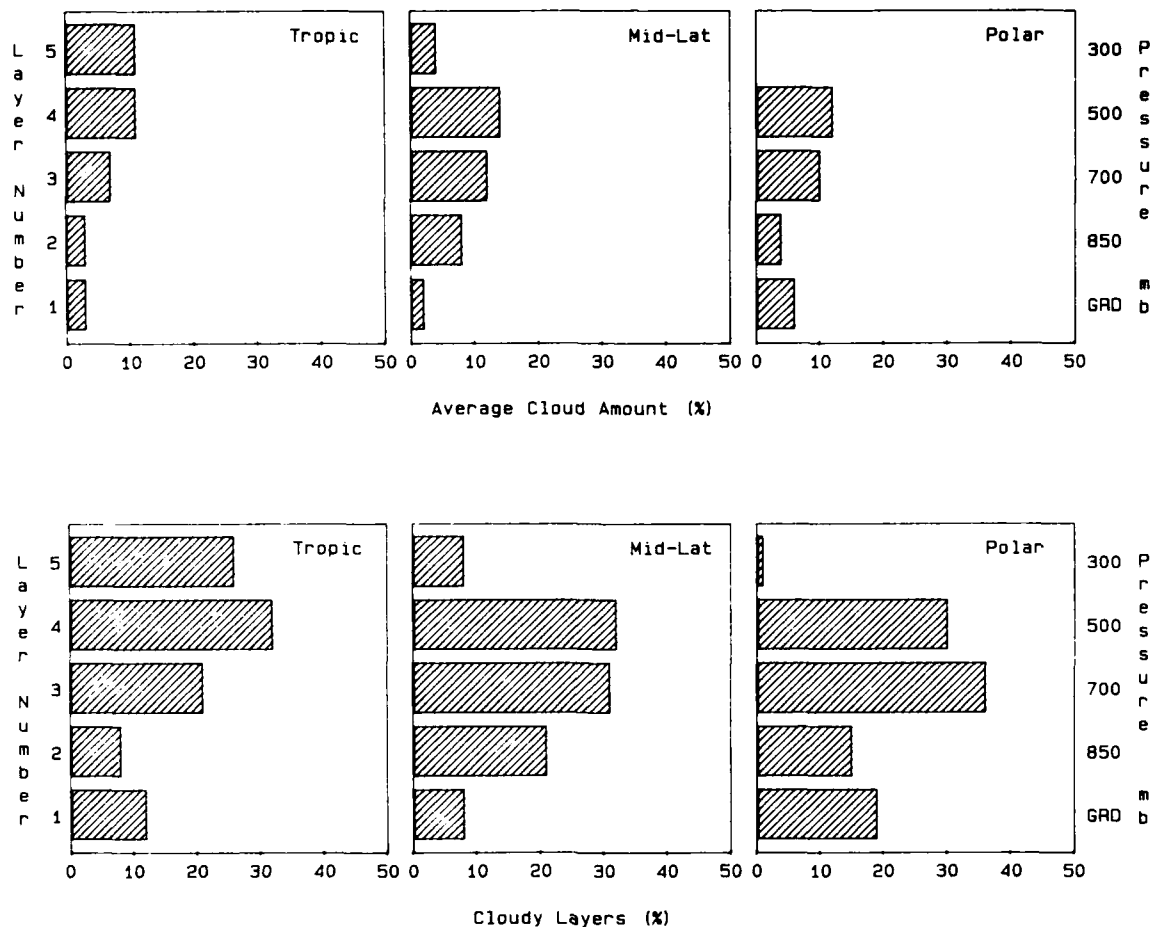


**Figure 11.** Plots of Hemispheric Cloud Layer Distributions and Average Layer Cloud Amounts as a Function of Height for the AFGL Algorithm, Winter Day 85009 (See Table 16)

The amount of low clouds at mid-latitudes differs from deBary and Moller (1963) since both RTNEPH and AFGL amounts increase with altitude. The RTNEPH and AFGL results are in remarkably close agreement as is evidenced by intercomparing Figures 10 and 11.

## 6. CONCLUSIONS AND RECOMMENDATIONS

A series of comparison tests were run between the RTNEPH and AFGL layer algorithms. Results show that the AFGL algorithm finds fewer cloud layers than the RTNEPH. Interactive interpretation of satellite pictures rarely indicates the presence of three or four cloudy layers within an eighth-mesh box. The AFGL algorithm is preferred since it is less likely to overestimate the number of cloud layers. The results



also suggest that the tendency of the RTNEPH algorithm to find more cloud layers than the AFGL algorithm is independent of cloud altitude and does not favor any cloud type.

The IR processors of both algorithms find similar cloud heights and amounts. The AFGL algorithm gives slightly higher heights and average cloud amounts in the highest altitude ranges. The RTNEPH tends to find significantly more cloud layers, but the layer distribution over height is very nearly the same as for AFGL. These results are interpreted as a tendency for the RTNEPH algorithm to find more structure in a cloud layer, and to find several slightly different cloud tops where the AFGL algorithm might find only one.

Results also show that the average cloud heights assigned by the AFGL algorithm are higher on average than those for RTNEPH. The RTNEPH cloud heights are used to place analyzed clouds within one of five layers in the 5LAYER cloud forecast model. Thus, a change in analyzed cloud heights will affect a change in how the 5LAYER moisture field is initialized, subsequently affecting the model results. The differences between the RTNEPH and AFGL cloud heights are small with respect to the 5LAYER layers, preliminarily indicating that a noticeable effect on the 5LAYER cloud forecast would not be observed.

When the cloud fields of the RTNEPH and AFGL algorithms are displayed as grayshades on the AIMS, they are remarkably similar. The clear and cloudy regions have identical shapes since the clear/cloud decision is the same for both algorithms. The cloud temperatures found by the AFGL algorithm are about one grayshade higher than the RTNEPH cloud temperatures, so that the AFGL cloud fields appear very slightly colder. They also appear more uniform since the AFGL algorithm gives fewer layers.

Although in general there is little difference between the RTNEPH and AFGL algorithms when the cloud tops are grouped into the 5LAYER layers, the RTNEPH tends to find an unrealistically larger number of cloud layers than AFGL. This results in a cloudier RTNEPH because of the upper cloud occlusion algorithm that is a part of the RTNEPH merge processor. The occlusion algorithm increases the cloud cover of the lower layers that were analyzed by the IR processor, because it assumes that they are obscured from satellite view by the higher layers. Thus, since RTNEPH finds more layers, it will generate an analysis that is more cloudy than the AFGL algorithm. In turn, the 5LAYER RTNEPH moisture initialization field is likely to contain higher humidity values than the AFGL field, hence affecting the 5LAYER cloud forecast.

To sum up, the AFGL algorithm gives a slightly more realistic cloud analysis at no additional computational cost. The comparison tests did not reveal any algorithm behavior that would harm the RTNEPH and it is recommended for global applications.

## 7. RTNEPH HEMISPHERIC DATABASE DISPLAYS

Full-color displays of the RTNEPH hemispheric databases (Figures 12 - 19) are presented on the following pages. Figure captions are self-explanatory, and list the section and page number where each figure is first referenced.

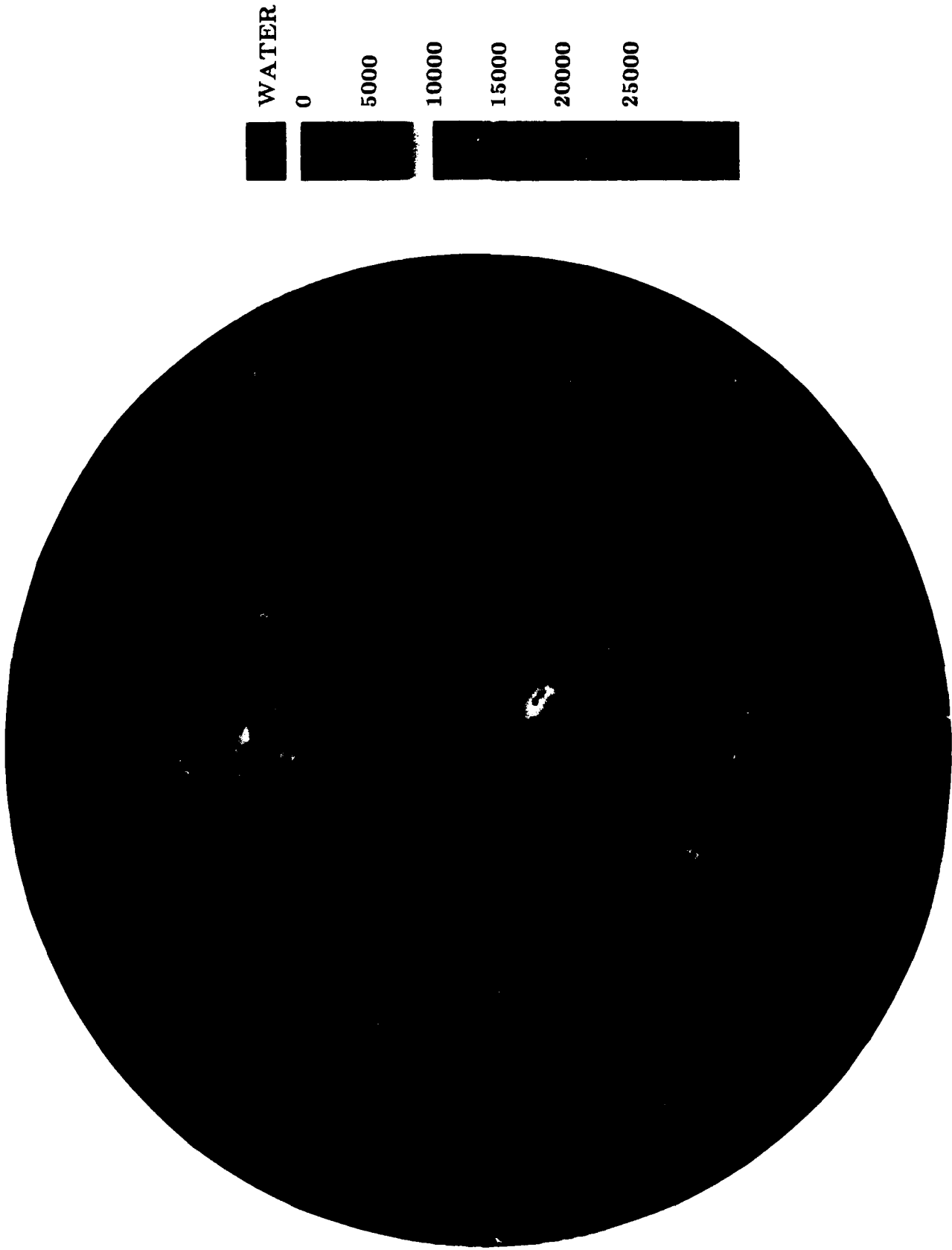
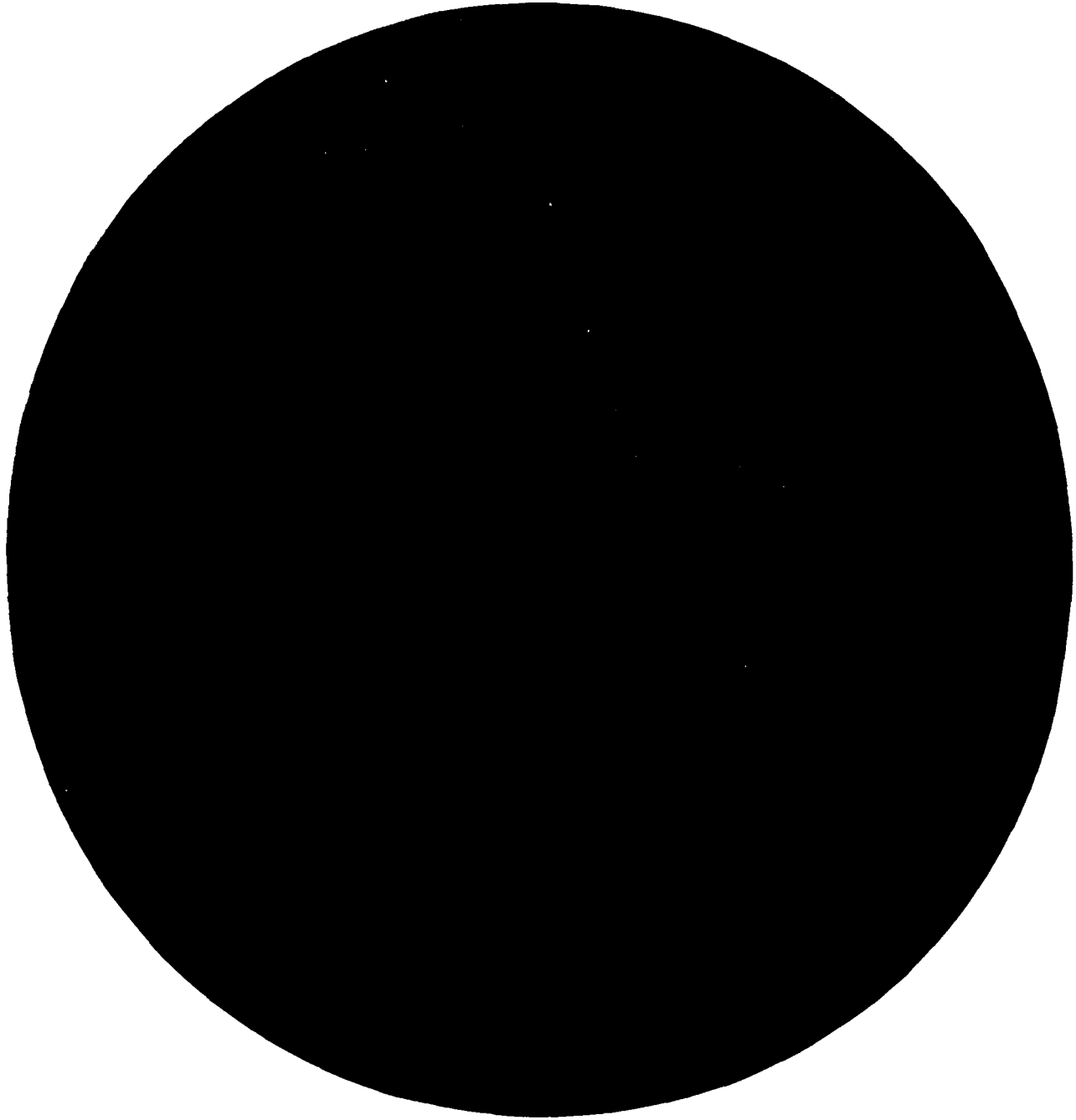


Figure 12. Northern Hemisphere Terrain Heights, in Feet ASL (See Section 3.1.1, Page 9)



WATER

LAND

COAST

ICE (BOTH)

ICE  
(82162 ONLY)

ICE  
(85010 ONLY)

Figure 13. Geography Flags for the Summer and Winter Case Study Days (See Section 3.1.1, Page 9)

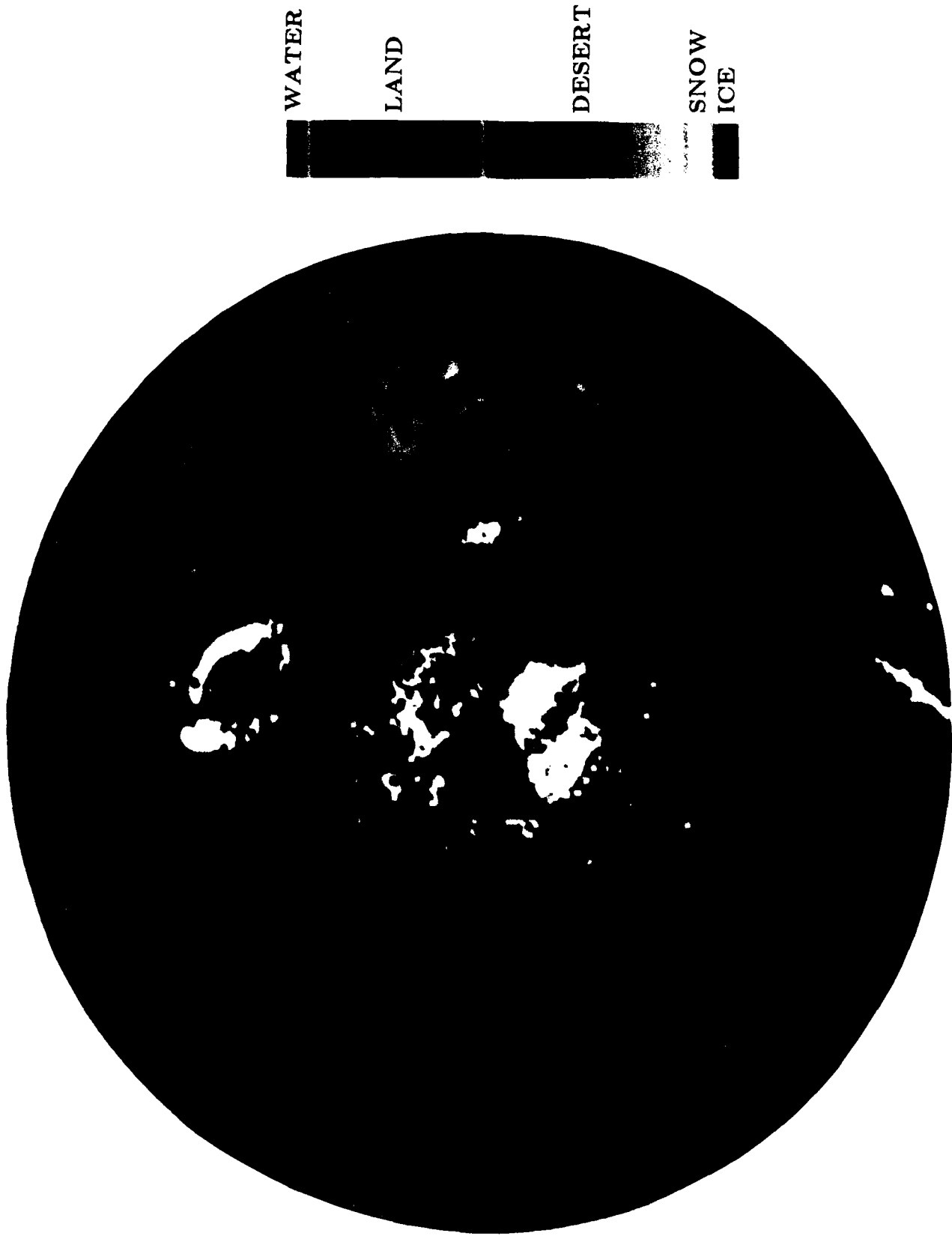


Figure 14a. Background Brightness for the Summer Day 82162 (See Section 3.1.1, Page 10)



WATER

LAND

DESERT

SNOW  
ICE



Figure 14b. Background Brightness for the Winter Day 85009 (See Section 3.1.1, Page 10)

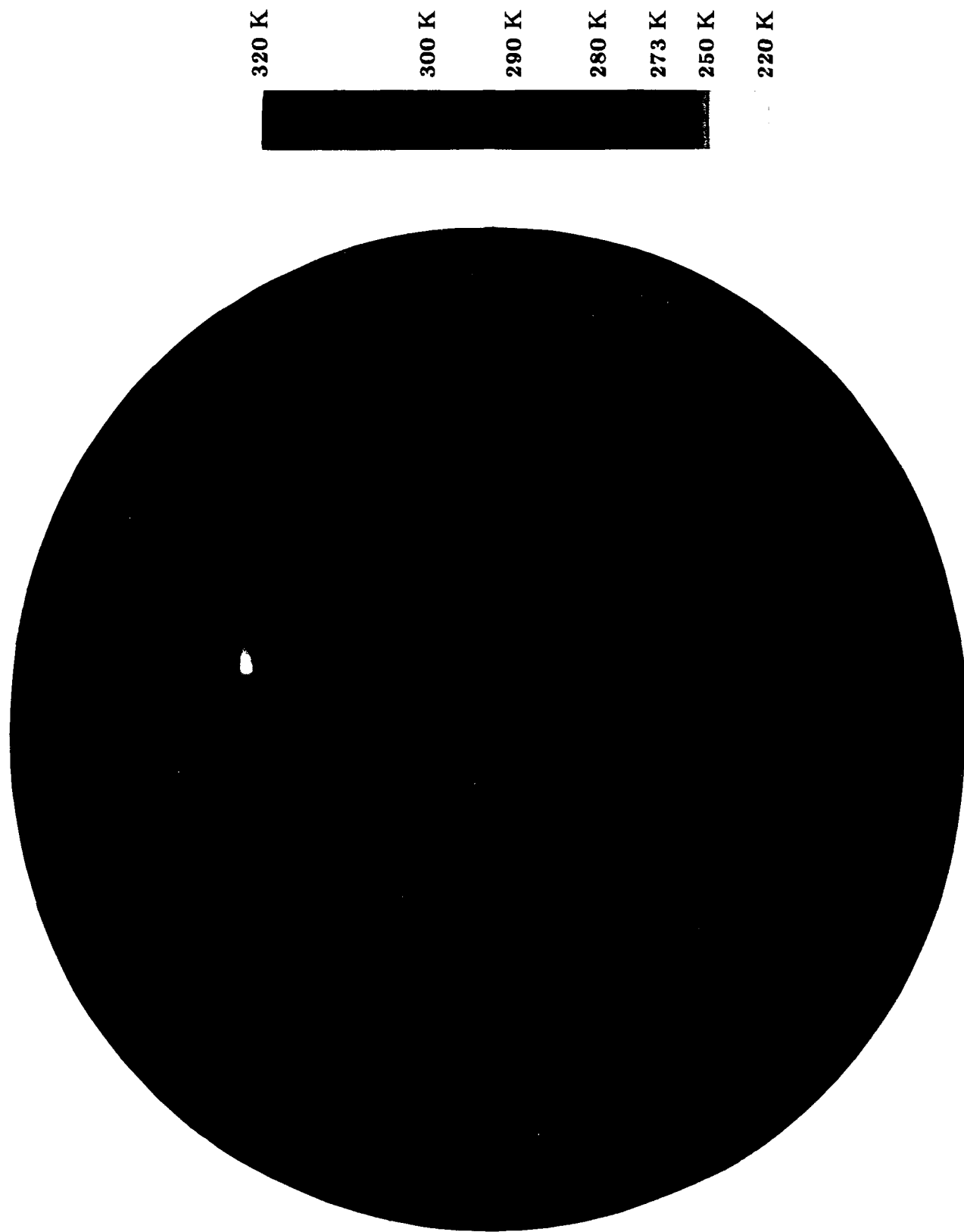


Figure 15a. Composite Surface Temperature Field for the Summer Case Study Day 82162 (See Section 3.1.1, Page 11)

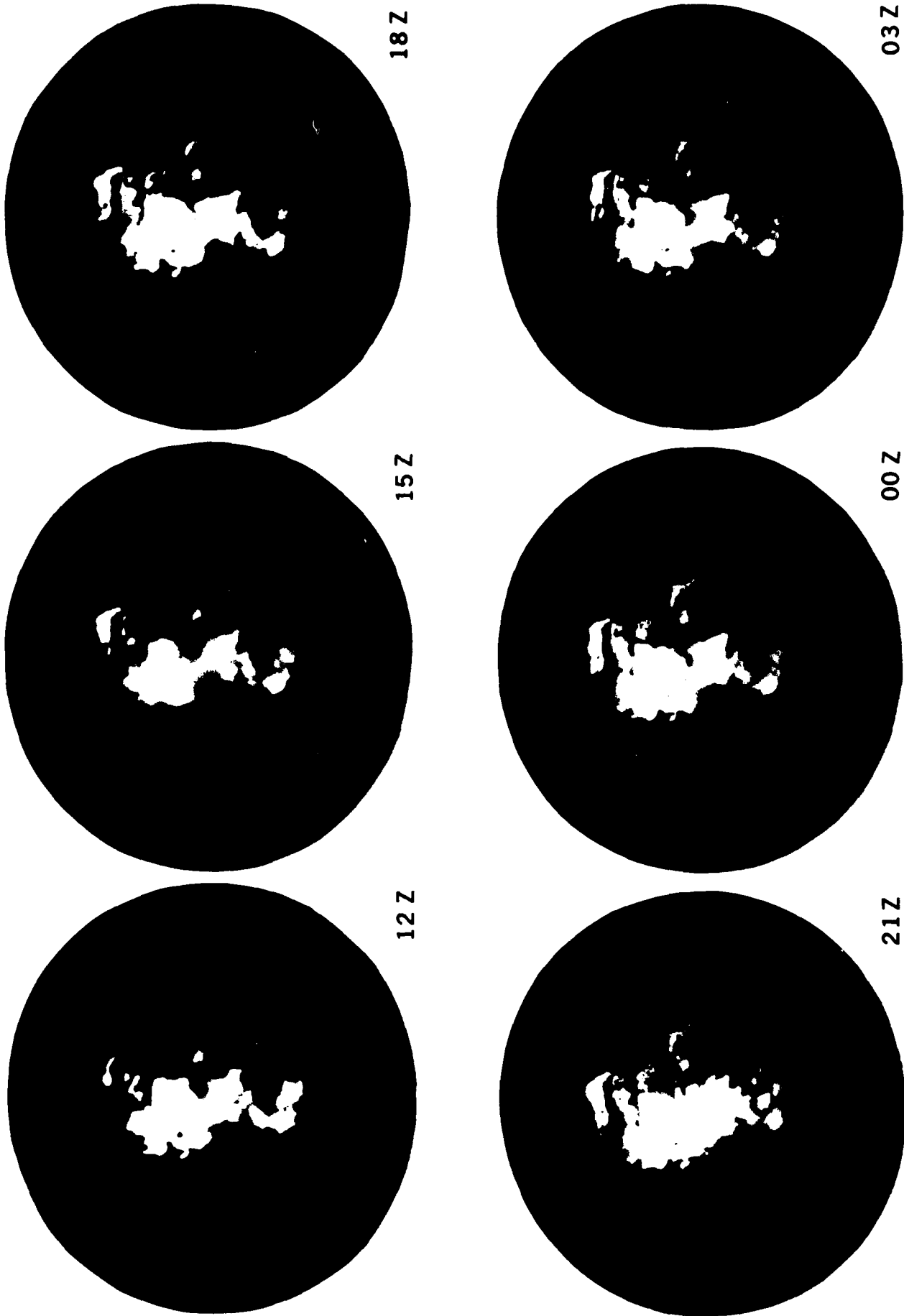


Figure 15b. Three-hourly Surface Temperature Fields for the Winter Case Study Day 85009 (See Section 3.1.1, Page 11)

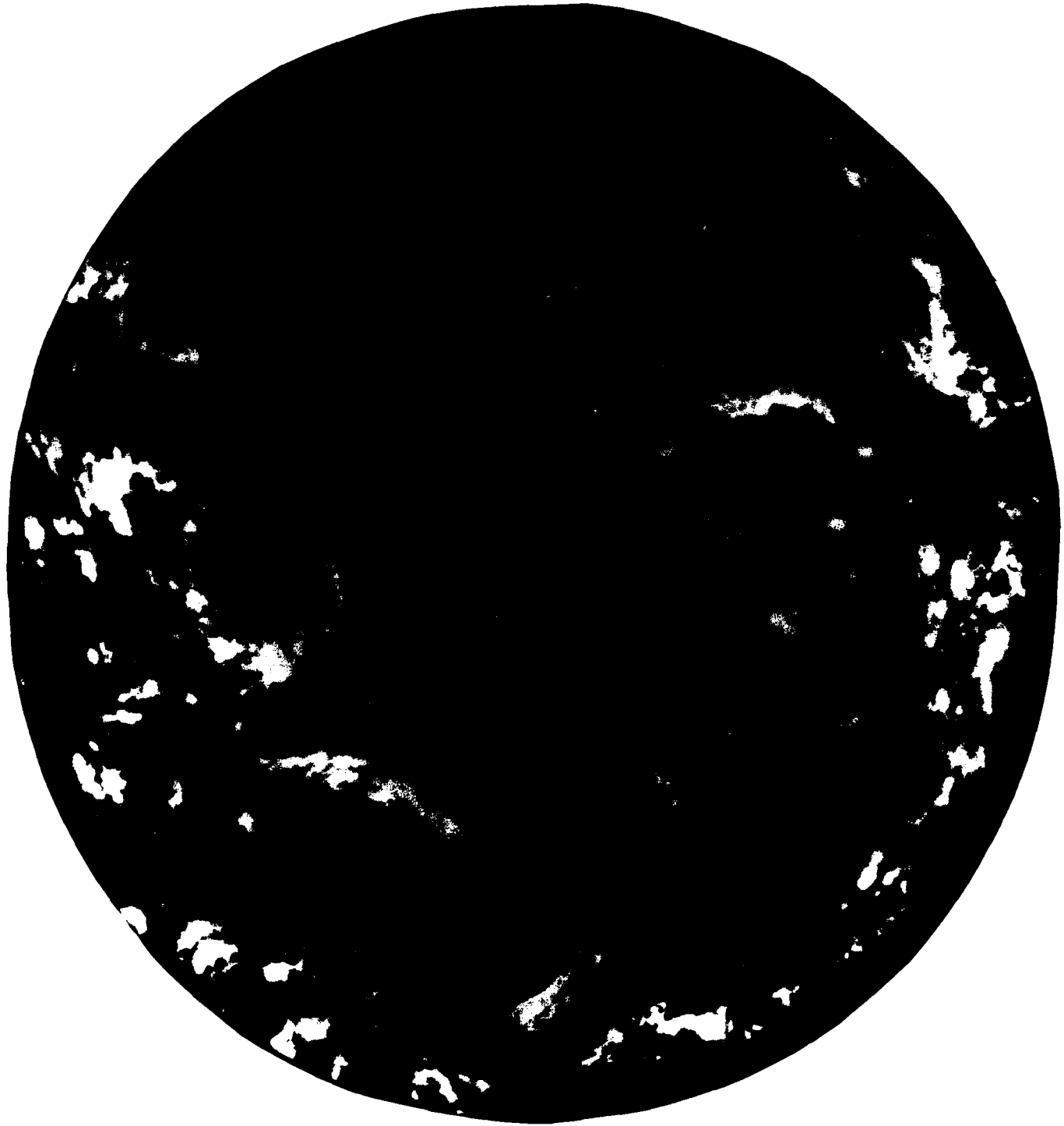




Figure 15c. Composite Surface Temperature Field for the Winter Case Study Day 85009 (See Section 3.1.1, Page 11)



**Figure 16.** Infrared Satellite Global Data Base Image for the Summer Case Study Day 82162 (See Section 3.1.2, Page 12)



**Figure 17.** Hemispheric Representative Grayshade Image for the Summer Case Study Day 82162 (See Section 4.1, Page 13)

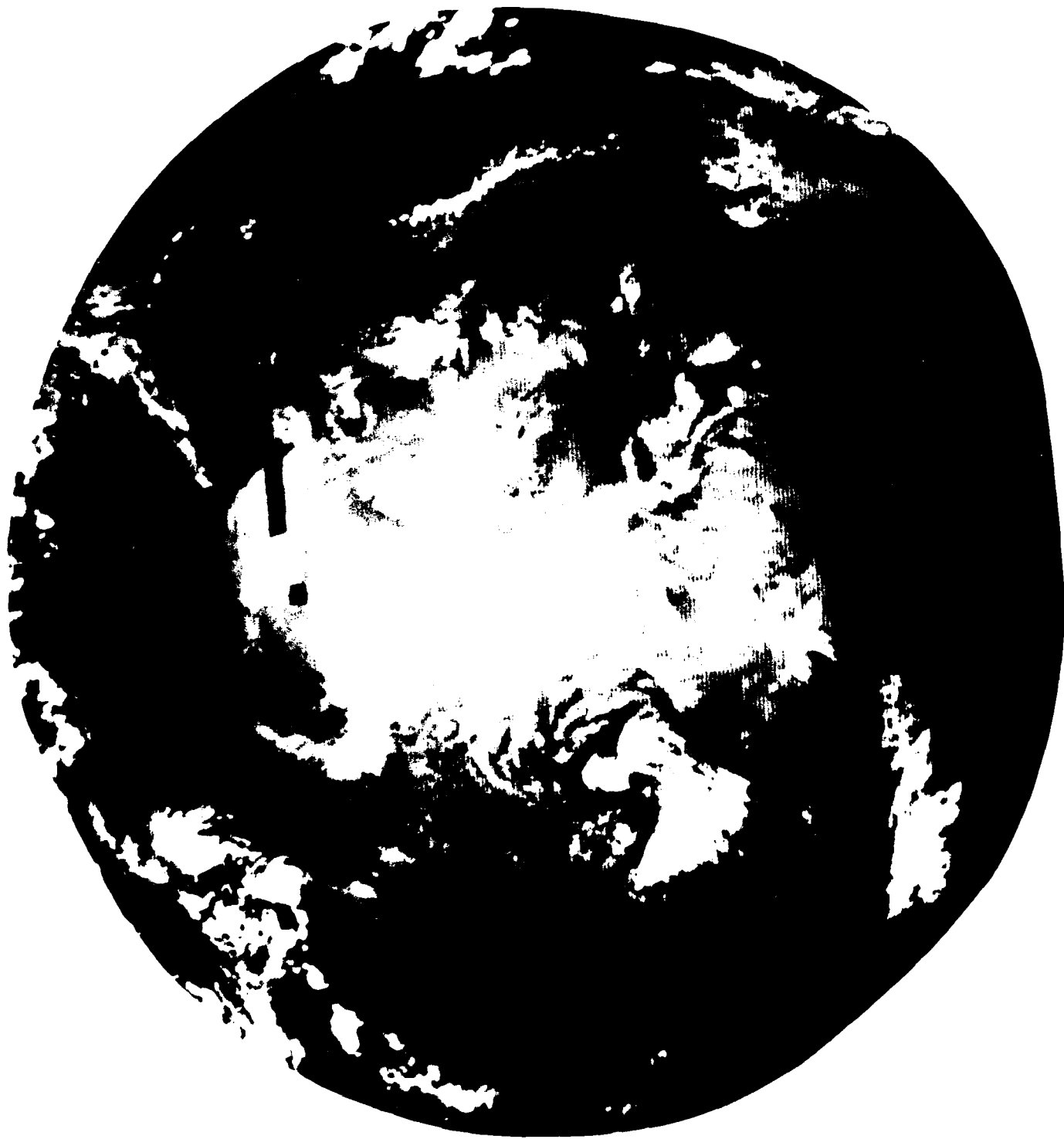


**Figure 18.** Infrared Satellite Global Data Base Image for the Winter Case Study Day 85009 (See Section 3.1.2, Page 12)



## 8. RTNEPH AND AFGL CLOUD ANALYSIS STATISTICS

RTNEPH and AFGL cloud analysis statistics are presented in Tables 7 - 16. Table captions are self-explanatory, and list the section and page number where each table is referenced.

Nephanalysis Infrared Processor Hemispheric Statistics — Summer — Day 82162								
Cloud Top Height Range: Low ( 0 — 2000 m )								
Background (# 1/8th-Mesh Boxes Processed)	Algorithm	Layer Frequency (%)				Ave. # of Layers Per 1/8 Box	Average Cloud Amount (%)	Average Cloud Height (m)
		1	2	3	4			
(17816) Land/Coast	RTNEPH	65	22	9	2	1.48	21	1324
	AFGL	72	25	1	0	1.29	17	1340
(98478) Water/Ice	RTNEPH	57	30	10	1	1.55	27	1108
	AFGL	66	32	1	0	1.35	24	1130
(116294) All Types	RTNEPH	59	29	10	1	1.54	26	1141
	AFGL	67	30	1	0	1.34	22	1161

Table 7. IR Processor Hemispheric Statistics for the Summer Case Study Day 82162, Low Clouds  
(See Section 5.1, pg. 27)

Nephanalysis Infrared Processor Hemispheric Statistics — Summer — Day 82162								
Cloud Top Height Range: Middle ( 2001 — 6000 m )								
Background (# 1/8th-Mesh Boxes Processed)	Algorithm	Layer Frequency (%)				Ave. # of Layers Per 1/8 Box	Average Cloud Amount (%)	Average Cloud Height (m)
		1	2	3	4			
(18923)	RTNEPH	33	22	23	19	2.32	49	3929
Land/Coast (18268)	AFGL	36	40	20	2	1.90	48	3946
(60553)	RTNEPH	54	14	18	12	1.89	33	3830
Water/Ice (58503)	AFGL	57	25	14	1	1.60	33	3857
(79476)	RTNEPH	51	15	19	13	1.97	36	3853
All Types (76771)	AFGL	54	28	15	2	1.66	36	3879

**Table 8.** IR Processor Hemispheric Statistics for the Summer Case Study Day 82162, Middle Clouds  
(See Section 5.1, pg. 27)



Nephanalysis Infrared Processor Hemispheric Statistics — Summer — Day 82162 Cloud Top Height Range: High ( 6001 — 22500 m )								
Background (# 1/8th-Mesh Boxes Processed)	Algorithm	Layer Frequency (%)				Ave. # of Layers Per 1/8 Box	Average Cloud Amount (%)	Average Cloud Height (m)
		1	2	3	4			
(8327)	RTNEPH	69	11	11	6	1.55	22	8927
Land/Coast (8308)	AFGL	70	17	10	1	1.42	23	9045
(26711)	RTNEPH	79	7	8	4	1.37	15	9417
Water/Ice (26711)	AFGL	80	12	6	0	1.28	16	9488
(35038)	RTNEPH	77	8	8	4	1.40	16	9298
All Types (35019)	AFGL	78	13	7	0	1.31	17	9381

**Table 9.** IR Processor Hemispheric Statistics for the Summer Case Study Day 82162, High Clouds  
(See Section 5.1, pg. 27)

Nephanalysis Infrared Processor Hemispheric Statistics — Winter — Day 85009								
Cloud Top Height Range: Low ( 0 — 2000 m )								
Background (# 1/8th-Mesh Boxes Processed)	Algorithm	Layer Frequency (%)				Ave. # of Layers Per 1/8 Box	Average Cloud Amount (%)	Average Cloud Height (m)
		1	2	3	4			
Land/Coast (60086) (64491)	RTNEPH	92	6	0	0	1.08	1	1351
	AFGL	95	4	0	0	1.05	1	1343
Water/Ice (105654) (114978)	RTNEPH	65	26	7	0	1.43	12	1045
	AFGL	75	23	0	0	1.25	9	1073
All Types (165740) (179469)	RTNEPH	75	18	5	0	1.31	8	1074
	AFGL	82	16	0	0	1.18	6	1097

**Table 10.** IR Processor Hemispheric Statistics for the Winter Case Study Day 85009, Low Clouds  
(See Section 5.1, pg. 27)

Nephanalysis Infrared Processor Hemispheric Statistics — Winter — Day 85009 Cloud Top Height Range: Middle ( 2001 — 6000 m )								
Background (# 1/8th-Mesh Boxes Processed)	Algorithm	Layer Frequency (%)				Ave. # of Layers Per 1/8 Box	Average Cloud Amount (%)	Average Cloud Height (m)
		1	2	3	4			
(20858) Land/Coast	RTNEPH	70	15	9	4	1.50	16	4032
(19856)	AFGL	71	23	4	0	1.34	15	4149
(39403) Water/Ice	RTNEPH	68	13	12	5	1.54	18	3811
(37266)	AFGL	70	22	6	0	1.37	19	3864
(60261)	RTNEPH	69	14	11	4	1.53	17	3885
(57122)	AFGL	71	22	6	0	1.36	17	3957

**Table 11.** IR Processor Hemispheric Statistics for the Winter Case Study Day 85009, Middle Clouds  
(See Section 5.1, pg. 27)

Nephanalysis Infrared Processor Hemispheric Statistics — Winter — Day 85009								
Cloud Top Height Range: High ( 6001 — 22500 m )								
Background (# 1/8th-Mesh Boxes Processed)	Algorithm	Layer Frequency (%)				Ave. # of Layers Per 1/8 Box	Average Cloud Amount (%)	Average Cloud Height (m)
		1	2	3	4			
(8516) Land/Coast	RTNEPH	88	5	4	1	1.18	8	8034
	AFGL	88	8	2	0	1.14	9	8119
(20263) Water/Ice	RTNEPH	84	7	5	2	1.26	12	8300
	AFGL	84	10	4	0	1.21	13	8381
All Types (28779)	RTNEPH	85	6	5	2	1.23	11	8227
	AFGL	86	9	3	0	1.18	12	8309

**Table 12.** IR Processor Hemispheric Statistics for the Winter Case Study Day 85009, High Clouds  
(See Section 5.1, pg. 27)

5-LAYER Layer # (Central Pressure)	Tropical		Mid-Latitude		Polar	
	Layer Distribution (%)	Cloud Amount (%)	Layer Distribution (%)	Cloud Amount (%)	Layer Distribution (%)	Cloud Amount (%)
1 (Gradient)	14	16	8	5	37	13
2 (850 mb)	18	18	22	16	37	12
3 (700 mb)	23	17	35	25	19	6
4 (500 mb)	27	19	23	15	7	2
5 (300 mb)	18	15	12	9	0	0

**Table 13.** Cloud Layer Distribution and Average Layer Cloud Amounts for the RTNeph Algorithm, Day 82162  
(See Figure 8; see also Section 5.1, pg. 27)

5-LAYER Layer # (Central Pressure)	Tropical				Mid-Latitude		Polar	
	Layer Distribution (%)	Cloud Amount (%)	Layer Distribution (%)	Cloud Amount (%)	Layer Distribution (%)	Cloud Amount (%)	Layer Distribution (%)	Cloud Amount (%)
1 (Gradient)	12	12	6	4	34	12		
2 (850 mb)	17	18	20	14	36	12		
3 (700 mb)	22	18	35	24	21	8		
4 (500 mb)	28	19	24	15	8	3		
5 (300 mb)	20	16	14	10	0	0		

**Table 14.** Cloud Layer Distribution and Average Layer Cloud Amounts for the AFGL Algorithm, Day 82162  
(See Figure 9; see also Section 5.1, pg. 27)

5-LAYER Layer # (Central Pressure)	Tropical		Mid-Latitude		Polar	
	Layer Distribution (%)	Cloud Amount (%)	Layer Distribution (%)	Cloud Amount (%)	Layer Distribution (%)	Cloud Amount (%)
1 (Gradient)	14	4	13	3	24	7
2 (850 mb)	10	3	23	9	15	4
3 (700 mb)	23	8	31	12	34	10
4 (500 mb)	30	11	28	13	26	12
5 (300 mb)	22	10	6	4	1	0

**Table 15.** Cloud Layer Distribution and Average Layer Cloud Amounts for the RTNEPH Algorithm, Day 85009  
(See Figure 10; see also Section 5.1, pg. 27)

5-LAYER Layer # (Central Pressure)	Tropical		Mid-Latitude		Polar	
	Layer Distribution (%)	Cloud Amount (%)	Layer Distribution (%)	Cloud Amount (%)	Layer Distribution (%)	Cloud Amount (%)
	1 (Gradient)	12	3	8	2	19
2 (850 mb)	8	3	21	8	15	4
3 (700 mb)	21	7	31	12	36	10
4 (500 mb)	32	11	32	14	30	12
5 (300 mb)	26	11	8	4	1	0

**Table 16.** Cloud Layer Distribution and Average Layer Cloud Amounts for the AFGL Algorithm, Day 85009  
(See Figure 11; see also Section 5.1, pg. 27)



## References

1. Bunting, J. T., R. S. Hawkins, R. P. d'Entremont, and G. B. Gustafson (1983): **R&D Nephanalysis at the Air Force Geophysics Laboratory.** *Proc. Fifth Conf. on Atmospheric Radiation*, Amer. Meteor. Soc., 272-275.
2. Crum, T. D. (ed.) (1987): **AFGWC Cloud Forecast Models.** *Air Force Global Weather Central Technical Memorandum AFGWC-TN-87-001*, Offutt AFB, NE 68113, 73 pp.
3. deBary, E. and F. Moller (1963): **The Vertical Distribution of Clouds.** *Journ. Appl. Meteor.*; 2, 806-808.
4. d'Entremont, R. P., R. S. Hawkins, and J. T. Bunting (1982): **Evaluation of Automated Imagery Analysis Algorithms for Use in the Three-Dimensional Nephanalysis Model at AFGWC.** *Air Force Geophysics Laboratory Technical Report AFGL-TR-82-0397*, Hanscom AFB, MA 01731-5000, 39pp., ADA131986.
5. Fye, Falko K. (1978): **The AFGWC Automated Cloud Analysis Model.** *Air Force Global Weather Central Technical Memorandum AFGWC-TN-78-002*, Offutt AFB, NE 68113, 97 pp.
6. Gustafson, Gary B., D. K. Roberts, C. F. Ivaldi, R. Schechter, T. J. Kleespies, K. R. Hardy, R. P. d'Entremont, G. W. Felde, and R. Lynch (1987): **The AFGL Interactive Meteorological System.** *Proc. 3rd Intl. Conf. on Interactive and Information Processing Systems for Meteorology, Oceanography, and Hydrology*, Amer. Meteor. Soc., 151-154.

7. Gustafson, Gary B. and G. W. Felde (1988): **Interactive Satellite Image Processing Applied to Cloud Detection.** *Proc. 4th Intl. Conf. on Interactive and Information Processing Systems for Meteorology, Oceanography, and Hydrology*, Amer. Meteor. Soc., 100-103.
8. Gustafson, Gary B. and G. W. Felde (1989): **Validation of Automated Cloud Detection From Microwave Imagery.** *Proc. 5th Intl. Conf. on Interactive and Information Processing Systems for Meteorology, Oceanography, and Hydrology*, Amer. Meteor. Soc., 379-386.
9. Hahn, C. J., S. G. Warren, J. London, R. M. Chervin, and R. Jenne (1982): **Atlas of Simultaneous Occurrence of Different Cloud Types Over the Ocean.** *National Center for Atmospheric Research Technical Memorandum NCAR/TN-201+STR*, Boulder CO, 212 pp.
10. Hall, F. F. Jr., M. J. Post, R. A. Richter, G. M. Lerfald and V. E. Derr (1984): **Cirrus Cloud Model.** Chapter 7, **Atmospheric Transmittance/Radiance: Computer Code LOWTRAN 6.** Air Force Geophysics Laboratory Technical Report AFGL-TR-83-0187, Hanscom AFB, MA 01731-5000, 58-67, ADA 137786.
11. Hawkins, Rupert S. (1980): **A Clustering Technique for Satellite Image Analysis.** *Proc. 8th Conf. on Weather Forecasting and Analysis*, Amer. Meteor. Soc., 115-118.
12. Hawkins, Rupert S. (1981): **Objective Analysis of Satellite Cloud Imagery.** *Proc. 1981 Intl. Geoscience and Remote Sensing Symposium*, IEEE Geoscience and Remote Sensing Soc., 1, 477-482.
13. Hoke, J. E., J. L. Hayes, L. G. Renninger (1981): **Map Projections and Grid Systems for Meteorological Applications.** Air Force Global Weather Central Technical Memorandum AFGWC-TN-79-003, Offutt AFB, NE 68113, 86 pp.
14. Izumi, Y. (1982): **A Study of Cirriform Clouds over Eleven USSR Stations.** Air Force Geophysics Laboratory Technical Report AFGL-TR-82-0384, Hanscom AFB, MA 01731-5000, 148 pp., ADA 130085.
15. Kiess, Raymond B. and William M. Cox (1988): **The AFGWC Automated Real-Time Cloud Analysis Model.** Air Force Global Weather Central Technical Memorandum AFGWC-TN-88-001, Offutt AFB, NE 68113, 82 pp.

16. Woodbury, G. E. and M. P. McCormick (1983): **Global Distribution of Cirrus Clouds Determined from SAGE Data.** *Geophys. Res. Lett.*, 10: p 1180.